People's Democratic Republic of Algeria

Ministry of Higher Education and Scientific Research

University M'Hamed BOUGARA- Boumerdes

Institute of Electrical and Electronic Engineering

Department of Power and Control Engineering

Project Report Presented in Partial Fulfilment of
the Requirements of the Degree of

'MASTER'

In **Power Engineering**

Option: **Power Engineering**

Title:

Maximum Power Point Tracking for Solar Water Pumping System Under Partial Shading Conditions

Presented by:

- **BOUAFIA Imad**
- **AZIOUNE Ahmed**

Supervisor:

Dr. AMMAR Abdelkarim

Co-Supervisor:

Dr. BELMADANI Hamza

June 2024

Dedication

With immense pleasure and heartfelt gratitude,
I dedicate this humble work to my beloved parents,
my dear brother, and sister.
All my family, friends,
and teachers from primary school to my last
year of university.

BOUAFIA Imad

I have a great pleasure to dedicate this modest
work to my beloved parents, my dear brother, and
sisters.
All my family, all my friends.
All my teachers from primary to this year.

AZIOUNE Ahmed

Acknowledgment

First of all, we are grateful to almighty ALLAH for giving us strength and ability to understand, learn and complete this project.

Secondly , we would like to thank our project supervisors, ***Dr. AMMAR Abdelkarim*** *and* ***Dr. BELMADANI Hamza*** *for all the help, assistance, and valuable feedbacks they offered us during the realization of this work.*

We also would like to pay our special regards to all the people who contributed in any way to the work presented in this thesis.

Abstract

This report presents innovative approaches to maximize the power output of photovoltaic (PV) systems for water-pumping applications based on BLDC motor, specifically addressing challenges posed by partial shading, which occurs when certain parts of the PV array are shaded while others are exposed to sunlight.

Traditional Maximum Power Point Tracking (MPPT) algorithms, such as the Perturb and Observe (P&O) method, have limitations when it comes to dealing with partial shading, as these algorithms struggle to accurately identify the global maximum power point (GMPP), which is important for achieving optimal power generation. To overcome these limitations, this work introduces advanced metaheuristic algorithms, including Particle Swarm Optimization (PSO), Grey Wolf Optimization (GWO), and the Marine Predator Algorithm (MPA), to robustly track the GMPP, thus ensuring optimal performance despite variations in solar exposure. Furthermore, the efficiency of each algorithm is compared using simulation models generated in MATLAB/Simulink, where the results demonstrate that these algorithms significantly improve power extraction under partial shading conditions.

keywords :

Phtovoltaic (PV), Brushless DC motor (BLDC), Maximum power point tracking (MPPT), Global maximum power point (GMPP), Perturb and observe (P&O), Particle swarm optimization (PSO), Grey wolf optimization (GWO), Marine predator algorithm (MPA).

List of Abbreviations and Terms

SWPS	Solar Water Pumping System
RSA	Reptile Search Algorithm
PV	Photovoltaic
P	Power [W]
V	Voltage [V]
I	Current [A]
MPP	Maximum Power Point
MPPT	Maximum Power Point Tracking
GMPP	Global Maximum Power Point
LMPP	Local Maximum Power Point
LPs	Local Peaks
GP	Global Peak
HC	Hill Climbing
IC	Incremental Conductance
STC	Standard Test Conditions [25°C, 1 sun]
P&O	Perturb and Observe
PSO	Particle Swarm Optimization
GWO	Grey Wolf Optimization
MPA	Marine Predator Algorithm
P_{max}	Maximum Power
V_{mpp}	Maximum Power Point Voltage
I_{mpp}	Maximum Power Point Current

EMI	Electromagnetic Interference
FF	Fill Factor
DC	Direct Current
AC	Alternative Current
PVG	Photovoltaic Generator
PVS	Photovoltaic System
I-V	Current-Voltage
IGBT	Insulated Gate Bipolar Transistor
VSI	Voltage Source Inverter
BLDC	Brushless DC
PSCs	Partial Shading Conditions
SI	Silicon
I_{sc}	Short Circuit Current
V_{oc}	Open Circuit Voltage
W_m	Rotor Speed
TL	Load Torque
Te	Electromagnetic Torque
EMF	Electromotive Force

Table of Contents

List of Figures

List of Tables

General Introduction

Human-driven growth in the world's population and dependence on fossil fuels have led to a dual threat of energy challenges and a climate crisis [1]. To find a solution to the aforementioned problems, many studies have called for the use of renewable energies.

Among all renewable energies, solar energy is particularly interesting because of its clean exploitation and valuable contribution for providing sustainable energy solutions and reducing the expected impacts of climate change [2]. Solar energy, harnessed through photovoltaic (PV) systems, is particularly well-suited for water pumping applications, where regions with no normal water stockpile need to pump water from underground or other water sources.

A standard solar photovoltaic water pumping system (PVWPS) has the potential to bring sustainable supplies of potable water to millions of people in developing countries, especially in remote villages and farms where it is not economically feasible to extend the national electrical grid [3]. In view of being reliant on solar power, PV's output is rated using three main points: insolation rate, load nature, and temperature [4].

In order to maintain the power from the sun's rays, photovoltaics need maximum power point tracking (MPPT) algorithms to regulate the power from photovoltaics, regardless of the state of the atmosphere. Partial shading conditions significantly impact the output power of photovoltaic systems due to imprecise tracking of the global maximum power point (GMPP). Under shading conditions, the characteristics of PV devices become multimodal, having several power peaks [5].

The rapid expansion of photovoltaic (PV) systems has led to the requirement for new efficient Maximum Power Point Tracking (MPPT) techniques. Conventional control approaches for MPPT often result in suboptimal performance. As a result, some metaheuristic algorithms such as particle swarm optimization (PSO), grey wolf optimization (GWO), marine predator algorithm (MPA), reptile search algorithm (RSA), ...etc. have been more commonly used as nearly optimal MPPT solutions.

The aim of this report:

In this report, a system is designed to maximize the power extracted from the PV array to feed the pump through variable MPPT algorthims, regardless of the level of solar insolation available. Most conventional MPPT strategies, such as Perturb and Observe (P&O), can perform poorly in partial shading conditions. As a result, the MPPT metaheuristic algorithms have been employed as effective substitutes. Furthermore, particle swarm optimization (PSO), grey wolf optimization (GWO), and marine predator algorithm (MPA), were simulated and discussed in this work. The main presented contributions are: The design of a stand-alone photovoltaic water pumping system, The use of a Brushless DC (BLDC) motor, a presentation and comparison of different MPPT algorithms (Traditional/Metaheuristic), including P&O, PSO, GWO, and MPA.

Report organization:

The research presented in this report is organized into four chapters and each chapter is summarized as follows:

- **Chapter 1**: This chapter provides a background and a general overview of photovoltaics and solar water pumping systems. These systems are classified based on power source, type of pump, type of motor, and MPPT algorithm. A brief description of the SWPS used in this study is presented at the end.

- **Chapter 2**: This chapter includes the description and modeling of the main components used in our SWPS, including PV arrangements, DC-DC boost converter, three-phase VSI inverter, brushless DC motor, and centrifugal pump.

- **Chapter 3**: In this chapter, a review of the most widely used maximum power point tracking algorithms (traditional/metaheuristic) for photovoltaic systems under partial shading conditions is presented.

- **Chapter 4**: The simulation and results of our SWPS are introduced under different scenarios, using the various algorithms discussed in Chapter 3.

1. State of The Art

1.1 Introduction

One of the possible uses for a solar PV generation system is pumping water, which naturally requires energy. Pumping water, is a necessity for a large section of the world's rural population who do not have access to the grid. Considering that most of these rural people live in warm tropical or subtropical climates, using solar energy is a desired way to meet their basic energy requirements [6].

In solar water pumping systems, it is essential to operate with the maximum available power from PV panels without being affected by the change in irradiance all day. However due to partial shading conditions, the power output of the PV array reduces significantly, and thus the efficiency decreases, the configuration complexity increases, and the cost increases [7].

1.2 Solar Energy

Solar energy is renewable, clean, and eco-friendly, making it a desirable source of electricity supply for industrial and domestic applications. It becomes the ideal option in distant locations where connecting to the grid is technically impractical, especially for water pumping systems used for irrigation, drinking, or eating [8]. Additionally, solar energy can help reduce greenhouse gas emissions and combat climate change by providing a renewable alternative to fossil fuels. It also offers energy independence and can help lower electricity bills in the long run.

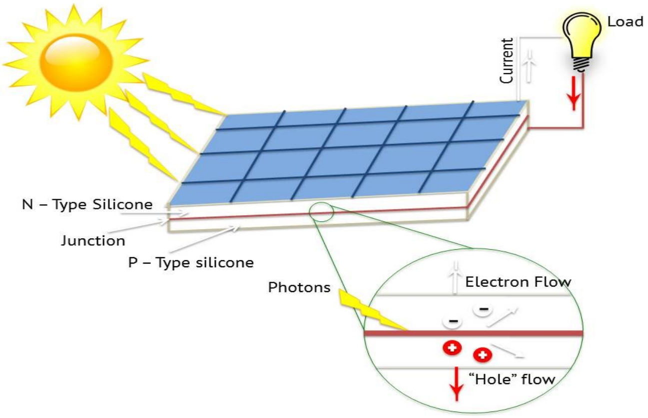

Figure 1.1. Photovoltaic energy transformation

As shown in the Figure 1.1, solar photovoltaic (PV) technology converts sunlight into electricity using PV effect that occurs when sunlight hits solar cells, creating an electric current by energizing electrons. Although, Solar energy is a renewable source with no fuel costs and low maintenance, but its initial installation costs can be very expensive [9].

1.3 Background of Solar Water Pumping System

1.3.1 Evaluation of SWPS

Today's many different kinds of applications highlight how mature solar photovoltaic (PV) technology has become. One of the most curious uses is the photovoltaic water pumping system (PVWPS), especially in areas where energy use from fossil fuels is not sustainable and connecting to the local grid is not always possible. Some important applications of this technology are for irrigation, community water supply, or hydro-energy storage systems [10].

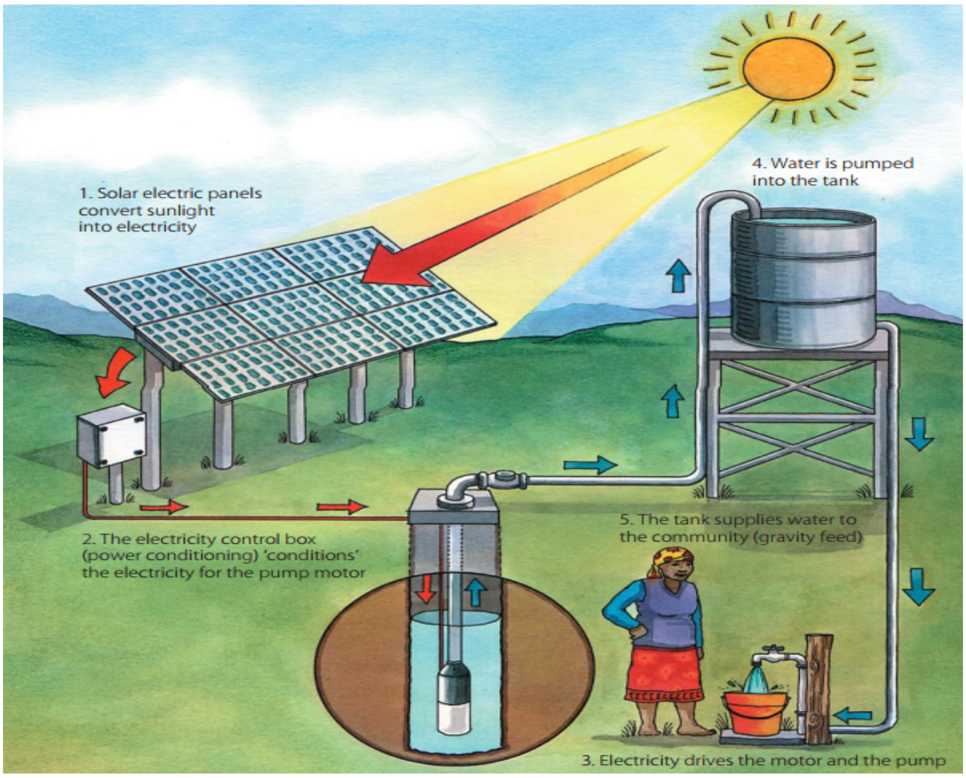

Figure 1.2. The basic configuration of SWPS

A generalized photovoltaic water pumping system (PVWPS) is presented in the Figure 1.2. It is composed of a water tank, a submersible or surface pump, a power conditioning unit, and a power collection system. PV panels, which accumulate solar energy and transform it into electrical energy, are the main component of the power collection system.

1.3.2 Solar Water Pumping Configurations

There are different types of solar water pumping systems, and we can distinguish between them using the following methods, depending on how they're classified:

1.3.2.1 Power Source Based SWPS

Solar energy provides the only power source for a stand-alone SPWS. It is comprised of a PV array that is connected by a controller to a pump assembly. A hybrid SPWS uses solar energy as its primary power source and connects an additional power source (such as grid power or AC power from a diesel generator) for pumping when solar energy is insufficient to run the pump.

• Stand-Alone battery-less Configuration

In a stand-alone battery-less SWPS, solar energy is the only power source. As shown in the Figure 1.3 below, it comprises a controller that joins a PV array, a pump assembly, and a storage tank which is usually installed alongside pumping equipment, allowing saved water to be used when SWPS shuts down.

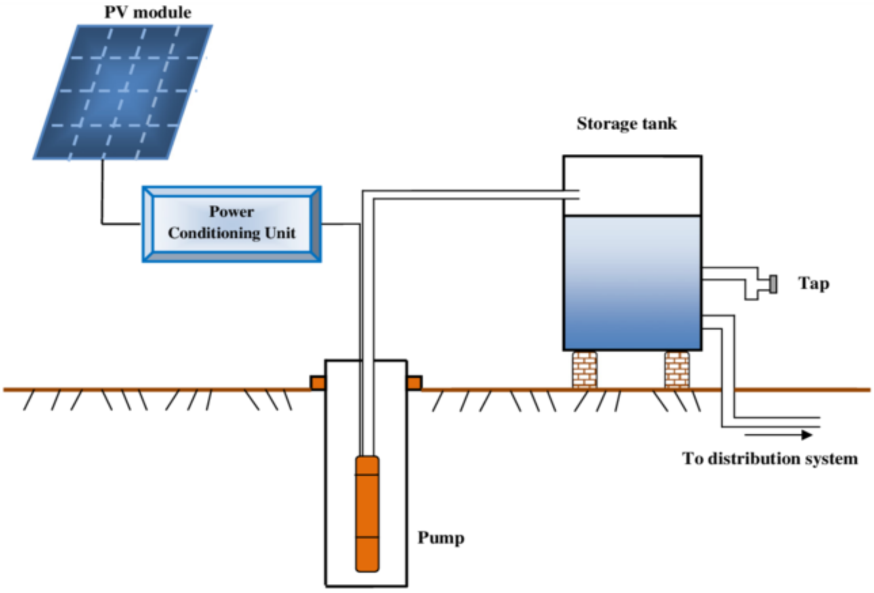

Figure 1.3. Schematic of stand-alone battery-less PV water pumping system

The solar stand-alone water pumping systems implementation may require careful consideration of site-specific conditions, water requirements, and cost-effectiveness compared to other alternatives. Furthermore, the system's efficiency can be affected by factors such as panel orientation, shading, and temperature [11].

The main drawbacks of a solar stand-alone water pumping system are the high upfront cost and the dependence on sunlight availability [12]. While, it offer a sustainable and renewable energy source.

• Hybrid Configuration

A hybrid photovoltaic water pumping system combines a battery bank with solar power [13]. The primary power source is a solar photovoltaic array, but it can utilize a battery bank when there is insufficient sunlight or during periods of high water demand [14].

In the hybrid configuration of SWPS, photovoltaic arrays and battery storage are used to ensure continuous water supply, overcoming low sunlight periods. The system, depicted in Figure 1.4, uses an advanced control algorithms to automatically switch between battery mode and normal mode based on sunlight changes in the region.

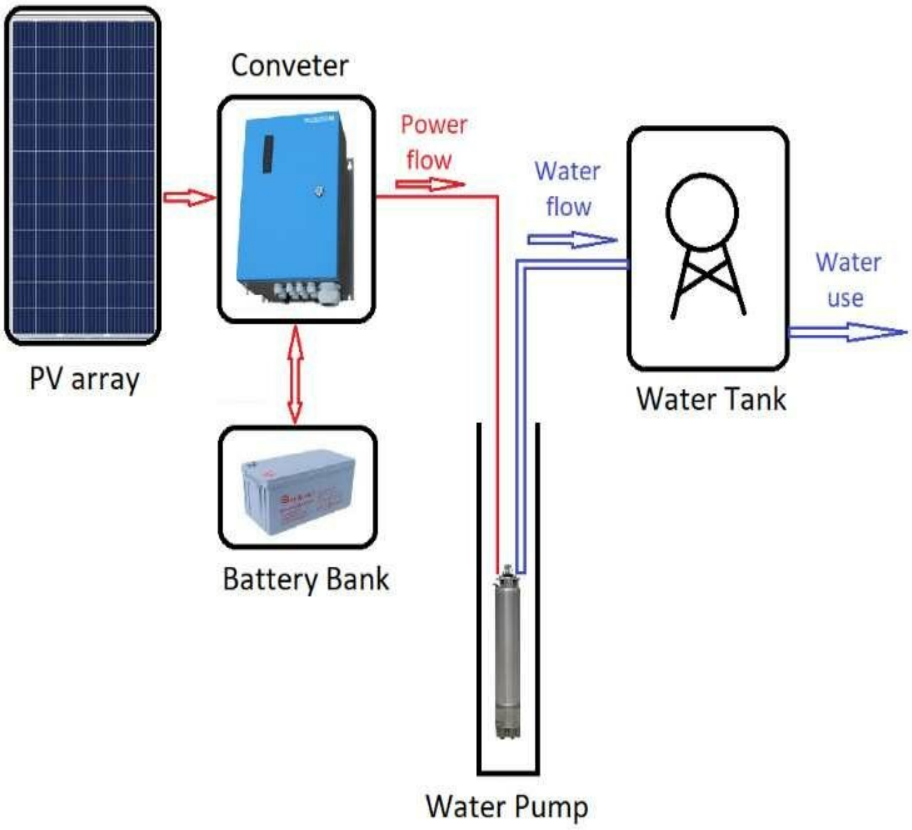

Figure 1.4. Schematic of hybrid solar PV water pumping system.

1.3.2.2 Based on Type of Pump (Water Source)

Three types of SWPS pumps are available including:

• Borehole/Well Pump (Submersible Pump)

As shown in the Figure 1.5, the solar water pump is located inside the well or borehole. These pumps are designed for boreholes measuring 100 mm (4 inches) and 150 mm (6 inches) where The water is normally pumped to a storage tank which is situated close to the top of the well or borehole. Typically, the pump controller is located next to the solar PV array, and waterproof cables are used to ensure its connection with the well pump [15].

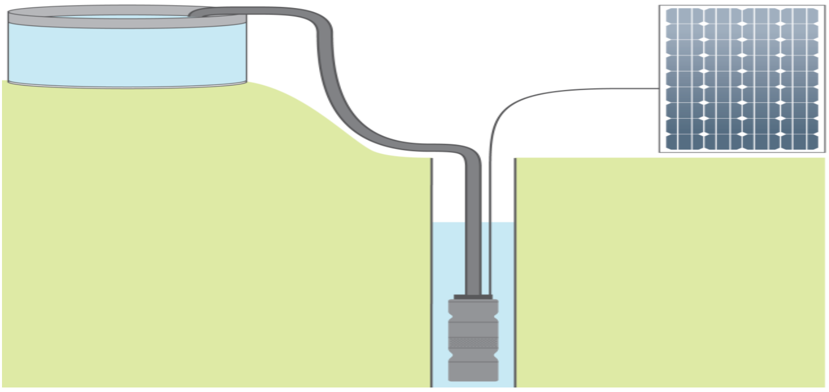

Figure 1.5. Borehole pump system

• Surface Pump

The surface pumps typically work in shallow wells or boreholes, lakes, rivers, and any other surface or nearby open water source. As illustrated below in the Figure 1.6, the solar pump is positioned above the water level, drawing water through a suction pipe from the water source. Their installation could take place in the Pacific, near rivers and streams, even though flooding could pose an important risk. It is unlikely that many sites connected to dams constructed especially for the pumping system will exist, though this might be the case for some larger irrigation water supplies [15].

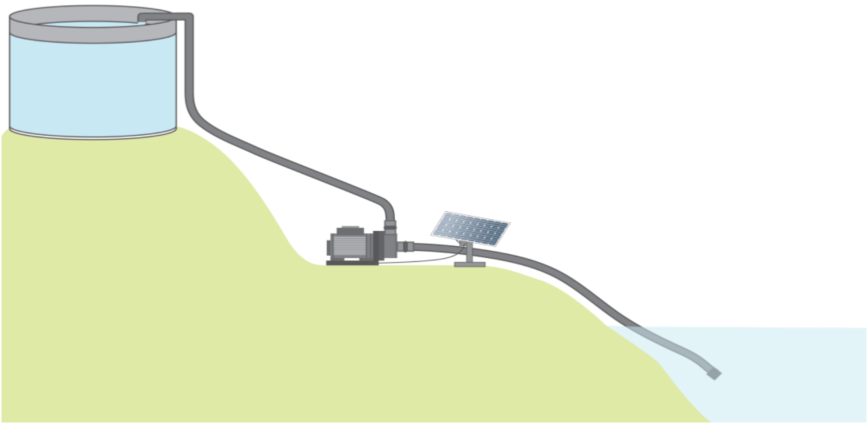

Figure 1.6. Surface pump system

- **Floating Pump**

For water extraction from large dams or open wells, the use of floating pumps is highly recommended. These pumps are mounted on a floating platform, ensuring that the pump's inlet remains submerged in water regardless of fluctuations in water levels. This design eliminates the need for a suction pipe and the associated complications. However, it necessitates the use of a flexible outlet pipe to accommodate variations in water levels over time. As shown in the Figure 1.7 below, the solar panels, which provide power to the pump, are typically installed on land in close proximity to the water source. The pumped water is generally directed to a storage tank or trough located at a distance from the water source. Furthermore, the pump controller is usually situated near the solar panels, with waterproof cables employed to connect it to the floating pump [15].

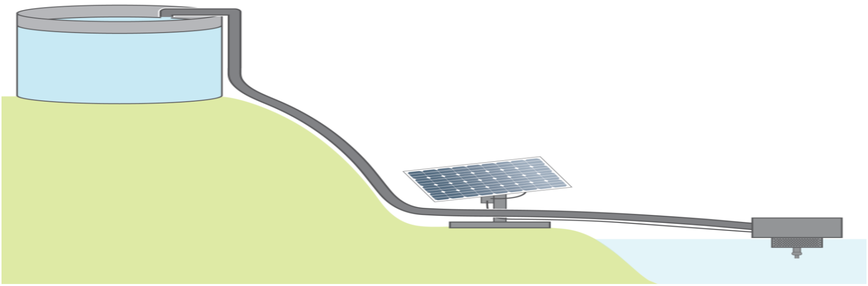

Figure 1.7. Floating pump system

1.3.2.3 Based on Type of Motor Used in SWPS

The equipment of the photovoltaic pumping subsystem must include electrical machines. They use a rotating shaft to convert electrical energy into mechanical energy. Solar pumping systems mainly use two types of motors: alternative-current (AC) motors and direct-current (DC) motors. As the motor is considered the heart of the system in SWP applications, SWPS can be classified into different categories depending on the type of motor to be used. These motors are categorized as illustrated in Figure 1.8.

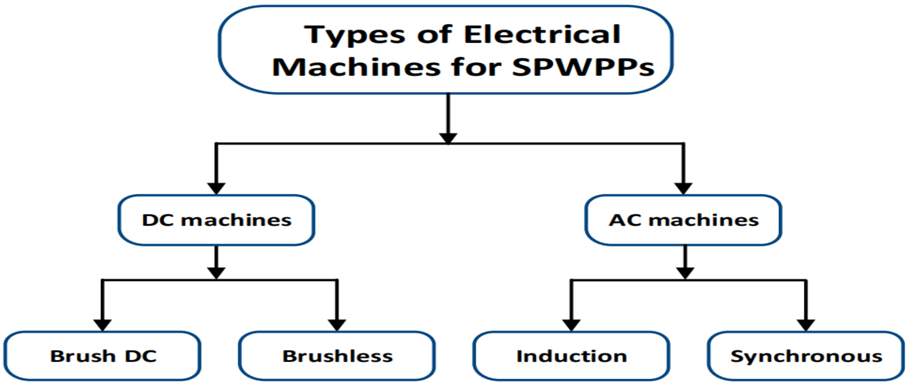

Figure 1.8. Main types of electrical machines for photovoltaic pump applications.

Table 1.1 below, presents a selection of research findings about the use of different motor drives for SWPS.

Table 1.1. Comparaison of different types of electrical machines

Machine Type	**Main results**
Brushless DC motor (BLDC)	• Dependable and efficient. • Offers precise torque and speed control. • Improves overall energy efficiency and adaptability to fluctuating water demands.
Brushed DC motor	• Requires more maintenance due to its mechanical commutation • More cost-effective and less complex.
Permanent Magnet Synchronous Motor (PMSM)	• Smaller size, higher speed, higher power density, longer lifespan, fewer sparks, and less audible noise. • Ideal for uses involving drives with adjustable speeds.
Induction Motor	• At high speeds, they are less likely to fail and are more robust. • Widely used because of their cost, accessibility, and durability. • The lack of brushes, commutators, and slip rings makes maintenance easier.

Due to the many characteristics that brushless DC motors provide such as: efficiency, speed-torque behavior, dynamic response, power density, and power factor, many people choose them for solar water pumping systems. With regard to operating under particular conditions, BLDC motors are a significantly more cost-effective and efficient option than other motors because of all these features.

• Brushless DC motor (BLDC)

In photovoltaic systems, brushless DC motors convert the electrical energy from PV panels into mechanical energy. Unlike brushed motors, BLDC motors use electronic commutation, eliminating the need for brushes. Brushless DC motors are favored because of their excellent efficiency, superior power density, lack of maintenance, lengthy lifespan, lack of electromagnetic interference (EMI) problems, and diminutive size [16].

However, they tend to be more expensive due to their complex construction and the need for sophisticated electronic controllers.

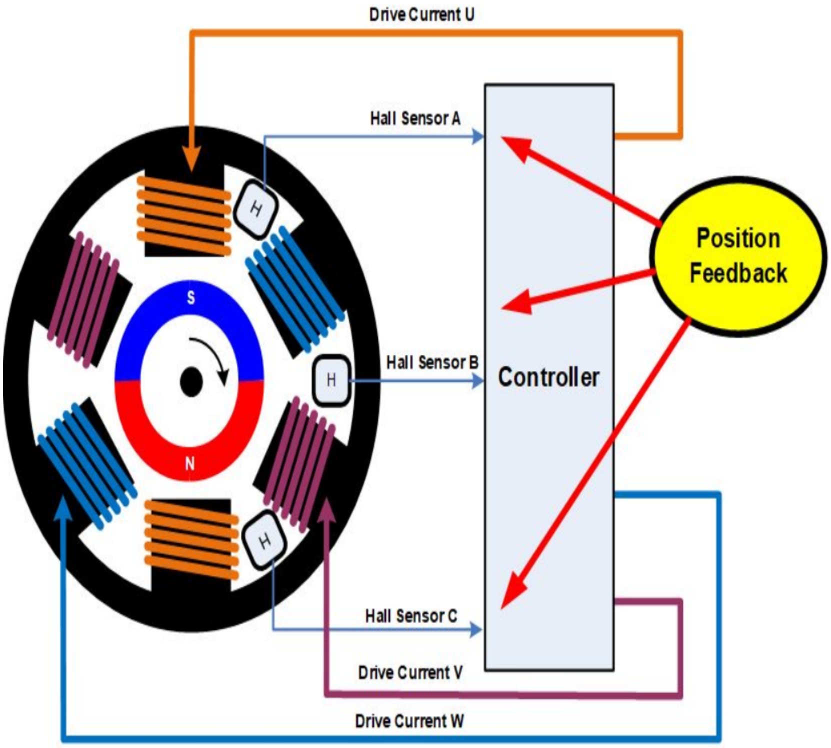

Figure 1.9. Brushless DC motor

This Figure 1.9 illustrates the control mechanism of a Brushless DC (BLDC) motor.

1.4 MPPT Algorithms

The first MPPT system was introduced in 1968 for a space system. Over the years, several MPPT algorithms have been developed and widely adapted to determine the maximum power point, mainly for applications in photovoltaic inverters. The most commonly used control techniques consist of acting automatically in the duty cycle, reaching the ideal point of the source, regardless of variations in weather conditions or sudden changes in loads, which can occur at any time [17].

The system operates as close to the voltage and current at the maximum power point (MPP), V_{mpp}, and I_{mpp}, respectively. The MPPT technique's fundamental idea is to match the conductance or resistance between the source and the load.

1.5 Solar Pumping System Description

The popularity of solar PV array-based water pumping systems that utilize boost converter-fed BLDC motors is due to their being highly efficient and eco-friendly [18]. A typical configuration of the solar-powered water pumping system is shown in Figure 1.10.

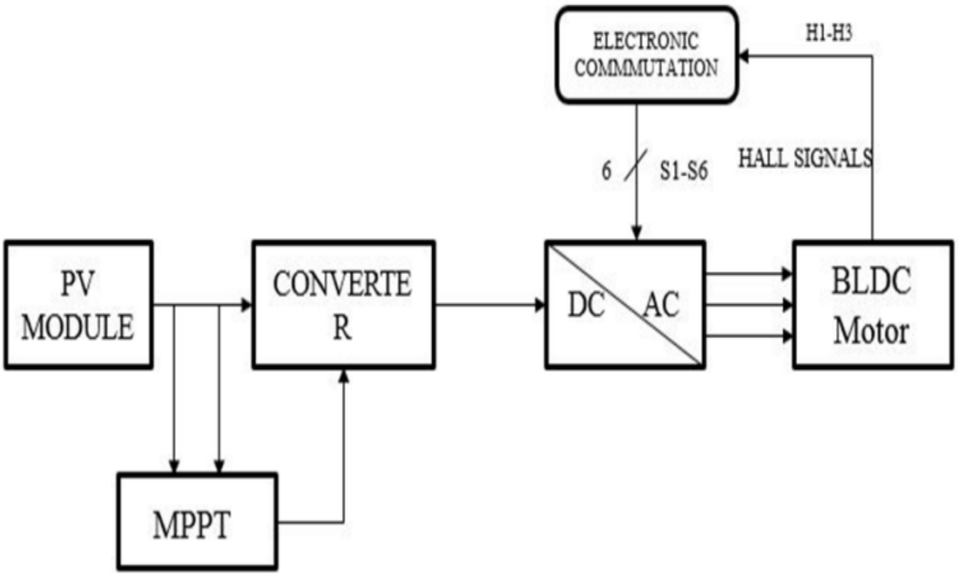

Figure 1.10. Block diagram of a solar water pumping system using a brushless DC (BLDC) motor

A solar PV array is one of the main parts of such a system, along with other parts like a boost converter, voltage source inverter (VSI), BLDC motor, and water pump.

In PV systems, the maximum amount of energy is extracted throughout the day by installing a DC/DC converter between a photovoltaic array and inverter. The maximum power point is extracted using Maximum Power Point Tracking (MPPT), an online control strategy that tracks the PVG's maximum output power operating point for varying climate conditions. MPPT is significant for SWPS because it lowers the cost of solar arrays by reducing the number of solar panels required to achieve the desired output power [19].

An inverter, which supplies a three-phase voltage has the ability to regulate the motor's speed based on the amplitude and frequency supplied. its implemention is necessary in order to operate the BLDC motor. This is dependent on the pump's water flow rate as well as variations in the weather.

1.6 Conclusion

By the end of this chapter, a general introduction to PV solar energy has been covered, and the significance of SWPS especially in remote or desert areas has also been demonstrated. Water pumping systems are categorized and identified according to their power source, which can be either standalone or hybrid, and are frequently utilized to increase system reliability. The water source forms the basis for a different classification, and the type of motor pump used in the system determines the final classification. Furthermore, a comparative analysis comparing the efficacy of various motors utilized in SWPS has been referenced to highlight the benefits of brushless DC motors over alternative motor types. By integrating MPPT into PV systems, especially in SWPS, the efficiency and reliability of the system can be significantly enhanced, ensuring a consistent water supply even under varying environmental conditions. Additionally, a general overview of the system was provided in the end.

2. System Configuration and Description

2.1 Introduction

The SPV array generates the electrical power required for the motor-pump. This electrical power is provided to the motor pump via a boost converter and a voltage source inverter (VSI). The SPV array appears as a power source for the boost converter as seen in Figure 2.1. Ideally, the same amount of power is delivered at the output of boost converter which appears as an input source for the VSI. In practice, because to the different losses associated with a dc–dc converter, slightly lower amount of power is delivered to feed the VSI. The MPPT algorithm needs voltage and current as feedback from SPV array and provides an optimal value of duty cycle to generate switching pulses for insulated gate bipolar transistor (IGBT) switch of the boost converter. In this way, the maximum power extraction and hence the efficiency optimization of the SPV array is accomplished. The VSI, converting dc output from a boost converter into ac, feeds the BLDC motor to drive a mixer grinder coupled to its shaft. The VSI is operated in fundamental frequency switching.

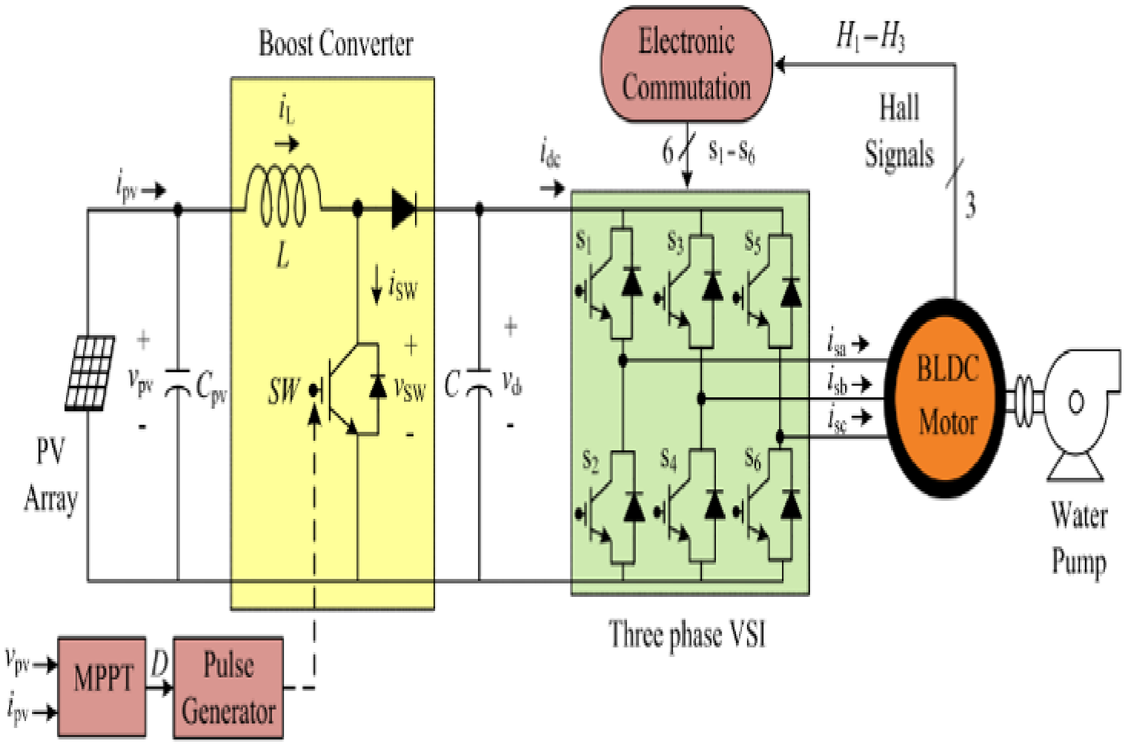

Figure 2.1. Configuration of the solar PV array and boost converter fed BLDC motor driven water pump

2.2 Photovoltaic Arrangements

2.2.1 Photovoltaic Cell

A photovoltaic cell is a material or electronic device that can convert the energy from photons of light into an electrical voltage and current. When photons (packs of solar energy from the sunlight) reach the photovoltaic cell, they are absorbed and hole-electron pairs will be generated. When these mobile charge carriers approach the p-n junction, the electric field in the depletion region will push the holes to move towards the p-side and the electrons to move towards the n-side, as seen in Figure 2.2. The p-side accumulates holes and the n-side accumulates electrons, which provides a voltage that may be utilized to send current to a load. If a load is placed between the negative and positive sides of the cell, the electrons flow as a current. More intense sunlight creates a greater current. If the light stops hitting the cell, the current stops flowing instantly [20]

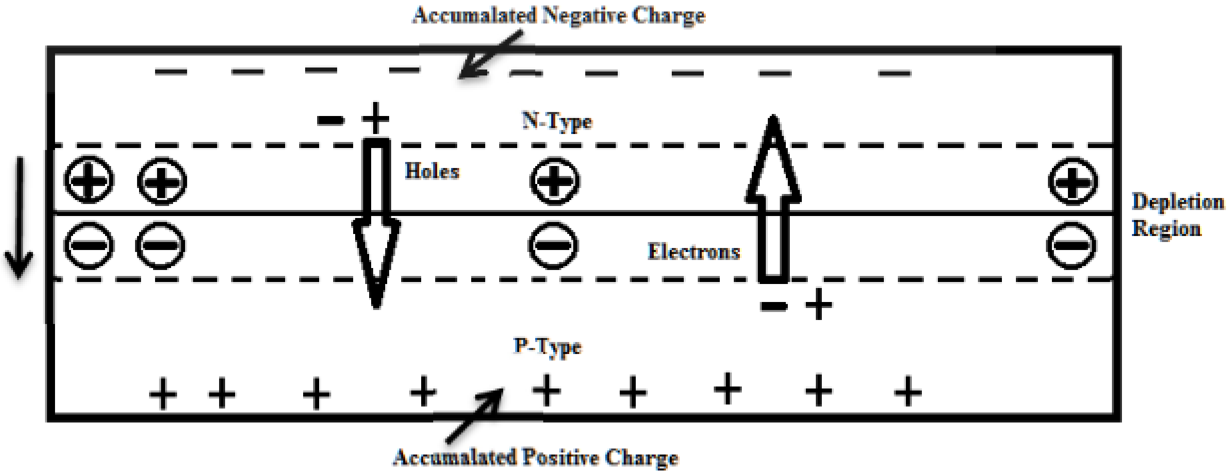

Figure 2.2. Function of a solar photovoltaic cell

When electrical contacts are attached to the top and bottom of the cell, electrons will flow out from the n-side into the connecting wire, through the load and they will be back to the p-side as shown in the Figure 2.3. Since wire cannot conduct holes, it is only the electrons that actually move around the circuit. When they reach the p-side, they recombine with holes completing the circuit. By convention, positive current flows in the direction opposite to electron flow, so the current arrow in the Figure 2.3 shows current going from the p-side to the load and back into the n-side [20].

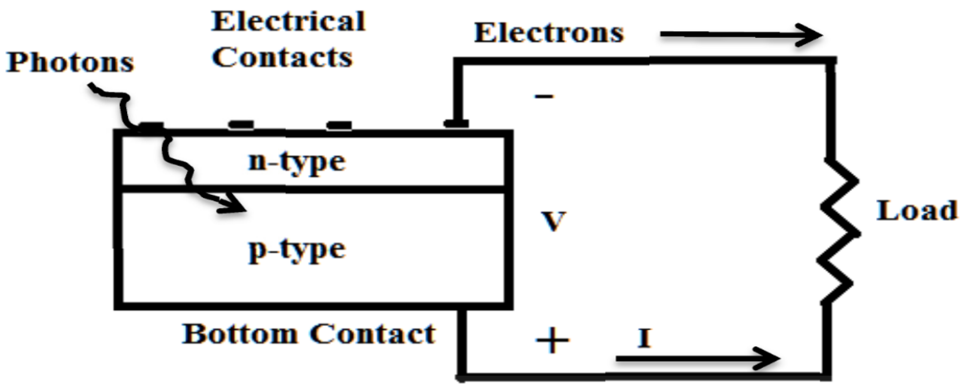

Figure 2.3. Flow of electrons and current through a photovoltaic cell

2.2.1.1 Solar Cell Connections

Connecting solar cells is similar to connecting batteries. When the positive terminal of one solar cell is connected to the negative terminal of another, a series connection is created. In this configuration, the current remains constant across all the cells, while the voltage is the cumulative sum of each cell's voltage, as depicted in Figure 2.4.

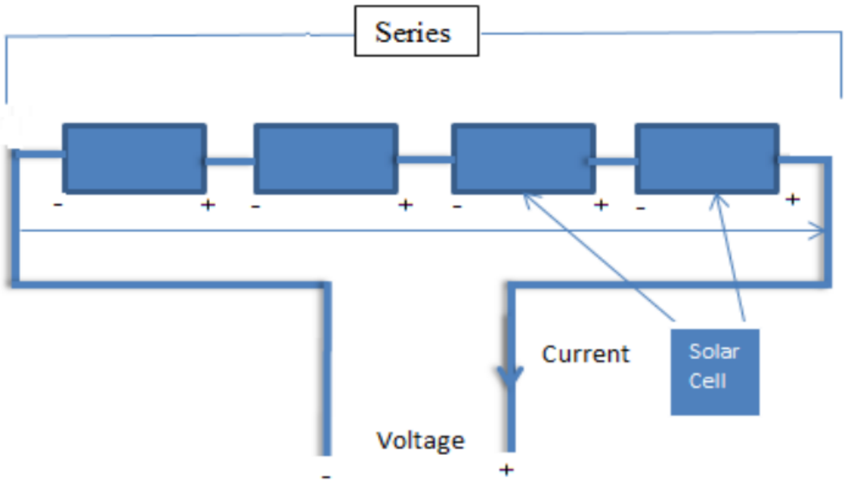

Figure 2.4. Series connection of solar cell

Alternatively, when all the positive terminals of the solar cells are connected to a common point and all the negative terminals are connected to another common point, a parallel connection is formed, as illustrated in Figure 2.5. In a parallel setup, the voltage across each cell remains the same, but the total current is the sum of the currents from each individual cell.

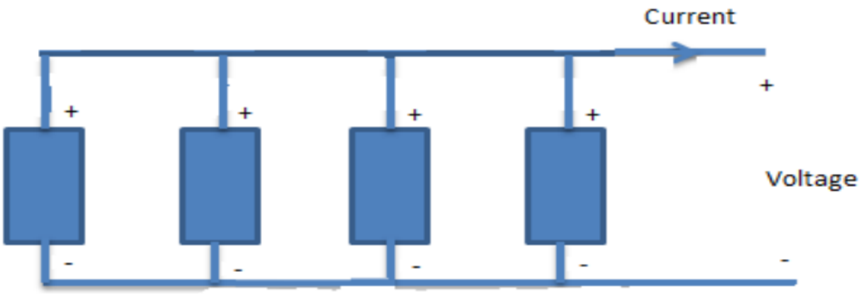

Figure 2.5. Parallel connection of solar cell

2.2.1.2 Model of PV Cell

In an ideal scenario, a solar cell is represented by a current source connected in parallel with a diode. However, real-world solar cells deviate from this ideal model due to imperfections. Consequently, additional components, such as shunt and series resistances Rsh and Rse respectively, are introduced into the model for greater accuracy, as shown in Figure 2.6 [21].

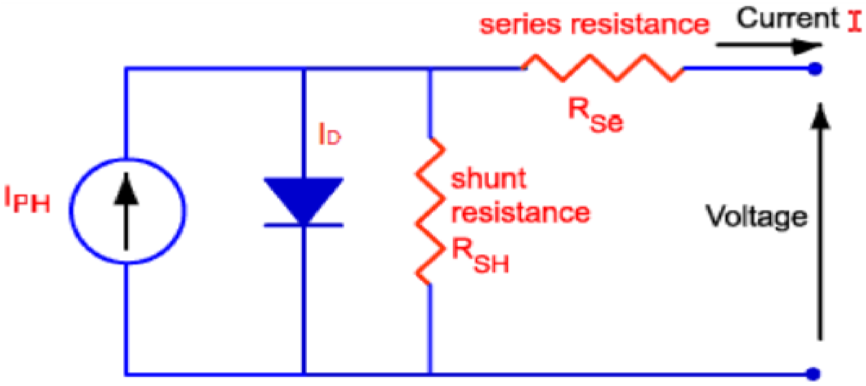

Figure 2.6. Equivalent circuits of solar cell

By applying node equation in Figure, where Iph, I_D, and I are meeting together, we get:

$$I_{ph} = I_D + I_{sh} + I \tag{2.1}$$

$$I = I_{ph} - I_D - I_{sh} \tag{2.2}$$

$$I = I_{ph} - I_{sat}.(e^{\frac{V+I.R_{se}}{V_T}} - 1) - \frac{V + I.R_{se}}{R_{sh}} \tag{2.3}$$

Where, I is the output-terminal current (A), I_{ph} is the current generated by solar cell (A), I_D is the diode saturation current (A), I_{sat} is the reverse saturation current of the diode (A), V is the Cell voltage (V), R_{se} is the Series resistance (Ω), R_{sh} is is the cell shent resistance (Ω), V_T is the Thermal voltage ($\frac{KT}{q}$), K is the Boltzman constant = 1.380649×10^{-23} (Joule/Kelvin), T is the rated cell Temperature (Kelvin) and q is the Charge of an electron = 1.68×10^{-19} (Coulomb).

2.2.1.3 PV Cell Curves

The electrical performance of a solar cell can be depicted by a specific graph known as the I-V curve, which stands for current-voltage curve. This graph effectively demonstrates how the cell behaves under varying conditions of temperature and sunlight intensity (irradiance). When a solar cell string is subjected to partial shading, the I-V curve will display changes in both current and voltage, thereby illustrating the impact of the shaded areas.

Under consistent irradiance and in the absence of any external obstructions, the I-V curve typically resembles the pattern shown in Figure 2.7, represented by a yellow line. This curve provides a clear view of the cell's operational characteristics under ideal conditions.

In the same figure, another important curve is presented, depicted by a blue line, and known as the P-V curve. This graph represents the power-voltage relationship and is crucial for understanding the amount of power being transferred to the load. The P-V curve also highlights the maximum power point (MPP) of the photovoltaic (PV) module, which is the point at which the module operates with maximum efficiency.

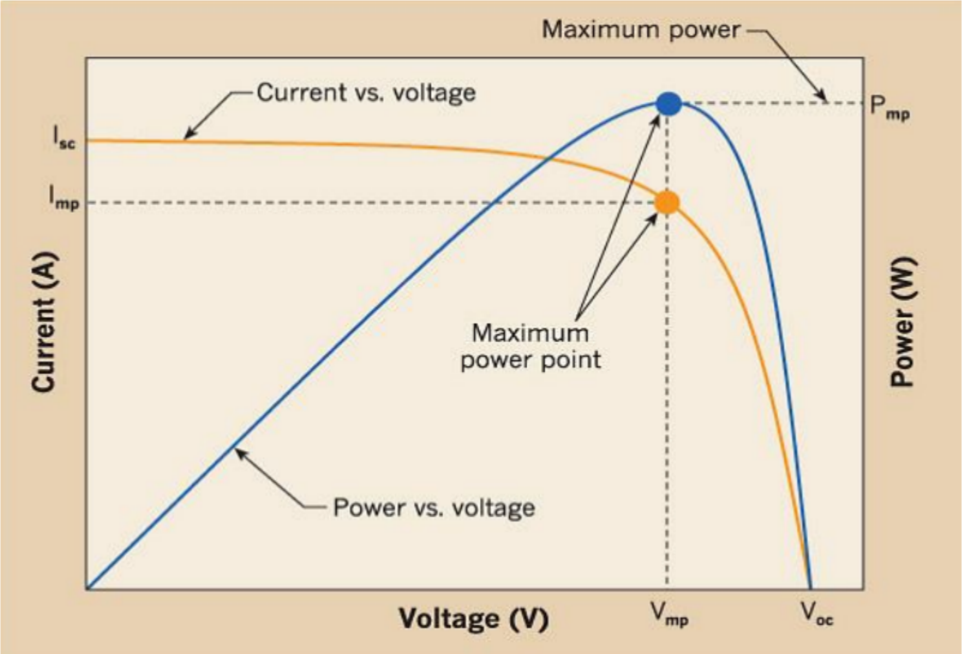

Figure 2.7. PV cell curves

The terms used in the Figure 2.7 are explained as follows:

- **Short Circuit Current** (I_{sc})**:** when zero load is applied to a PV device (resistance=zero),the device generates maximum current and zero voltage,reffered to as its short circuit current (I_{sc}).

- **Open Circuit Voltage** (V_{oc})**:** When zero load is attached to a PV device, it generates maximum voltage and zero current, known as its open circuit voltage (V_{oc}), resulting in zero output power

- **Maximum Power** (P_{max})**:** refers to the highest amount of power that a solar cell can produce under given environmental conditions, such as specific levels of sunlight and temperature. On the I-V curve, there exists a particular point where the product of current (I_{mp}) and voltage (V_{mp}) reaches its peak value. This crucial point is known as the Maximum Power Point (MPP).

- **Fill Factor (FF):** Indicates to the percentage value of maximum power to the total power produced by Voc and Isc and it is computed using the following formula:

$$FF = \frac{V_{mp} \times I_{mp}}{V_{oc} \times I_{sc}} \tag{2.4}$$

2.2.2 Photovoltaic Module & Array

A single photovoltaic (PV) cell generates a relatively low voltage of around 0.5 volts. To achieve higher voltage or current, multiple PV cells are combined in different configurations, such as series, parallel, or a combination of both, forming a PV module as depicted in the Figure 2.8. Furthermore, Standard PV modules typically contain either 36 or 76 cells.

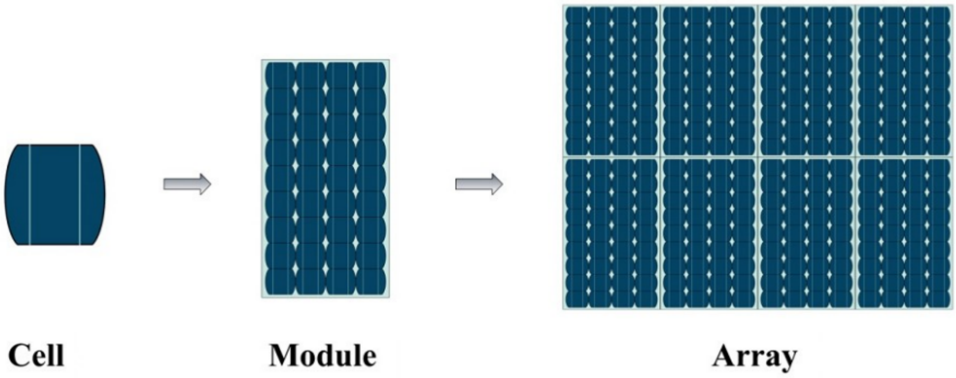

Figure 2.8. Photovoltaic system

In addition, a photovoltaic (PV) array is essentially a system where multiple PV modules are interconnected as illustrated in the Figure 2.8. Where, the connection of PV modules in an array mirrors the connection of cells within a single module. Furthermore, during the construction of a PV array, modules are initially connected in series to obtain the necessary voltage. These series connections are then linked in parallel to increase the current, based on specific requirements.

2.2.3 Effect of Variation of Solar Irradiation

The P-V and I-V characteristics of a solar cell are significantly influenced by the levels of solar irradiation. Due to environmental variations, solar irradiation fluctuates. However, various control mechanisms are used to monitor these changes and adjust the solar cell's operation to meet the required load demands. As illustrated in the Figure 2.9, with the increase of solar irradiation, the solar input to the cell also rises, leading to a higher power output for the same voltage. Similarly, with the increase of solar irradiation, the open circuit voltage also increses. This is because more sunlight hitting the solar cell provides electrons with higher excitation energy, which enhances their mobility and results in greater power generation.

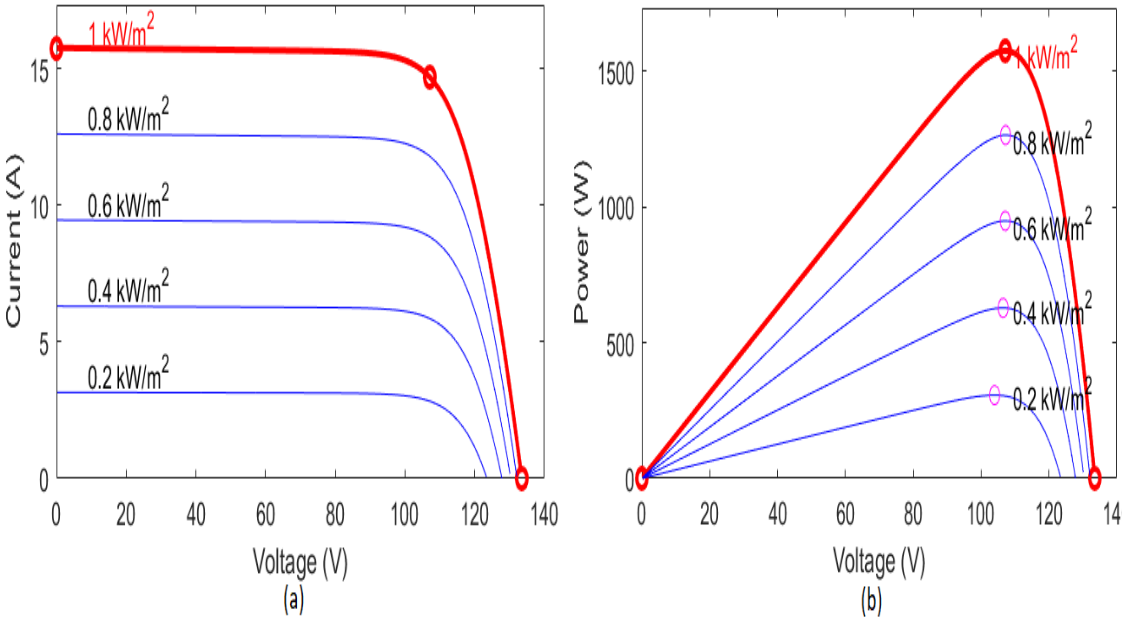

Figure 2.9. (a) I-V and (b) P-V characteristics of PV array under different levels of solar irradiation at 25°C

2.2.4 Effect of Variation of Solar Temperature

Conversely, a rise in temperature around the solar cell negatively affects its power generation capability. As the temperature increases, the open circuit voltage decreases, as depicted in the Figure 2.10. Higher temperatures cause an increase in the material's band gap, requiring more energy to overcome this barrier. Consequently, the efficiency of the solar cell reduces.

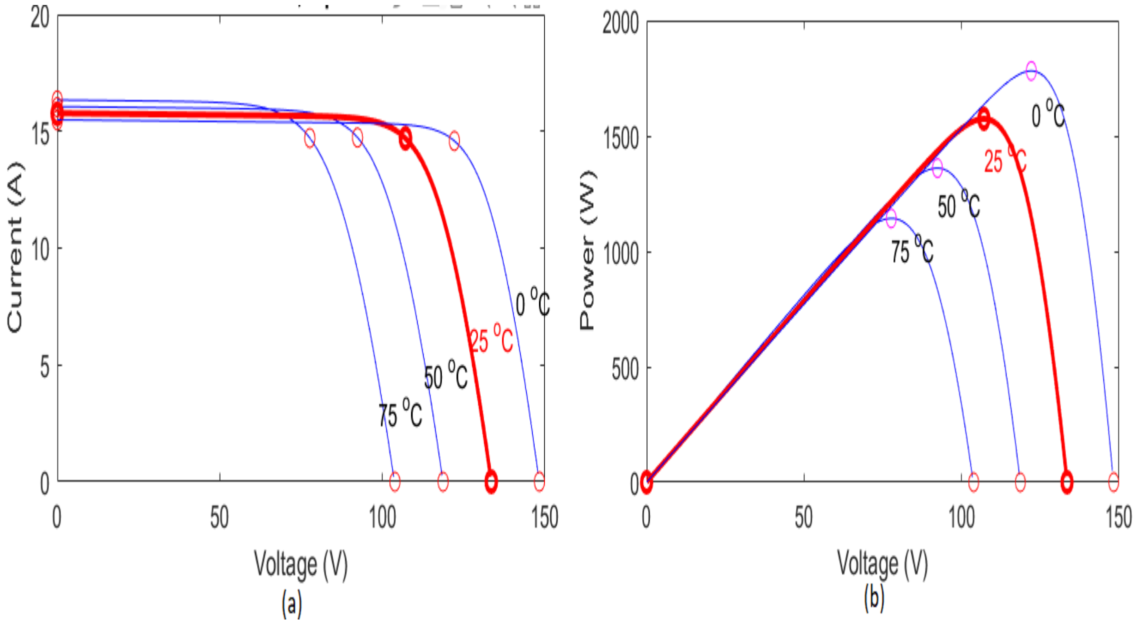

Figure 2.10. (a) I-V and (b) P-V characteristics of PV array under different temperatures at 1000 W/m^2

2.3 DC-DC Boost Converter

A DC/DC converter is a crucial component of any Maximum Power Point Tracking (MPPT) system. Without it, designing an MPPT circuit is impossible as directly connecting the source to the load causes the PV module's output to deviate from the maximum power point. To address this issue, an adaptation circuit must be placed between the source and the load [22]. Typically, an MPPT controller circuit with a DC-DC converter is installed between the PV array and the inverter to ensure a constant DC voltage at the generator's output [23].

In a boost converter or regulator, the output voltage is higher than the input voltage, hence the name "BOOST" regulator. The boost circuit as shown in the Figure 2.11, includes a DC input voltage source (V_{pv}), an energy-storing inductor (L), a capacitor (C), a diode (D), a load resistance (R), and a controlled switch (S).

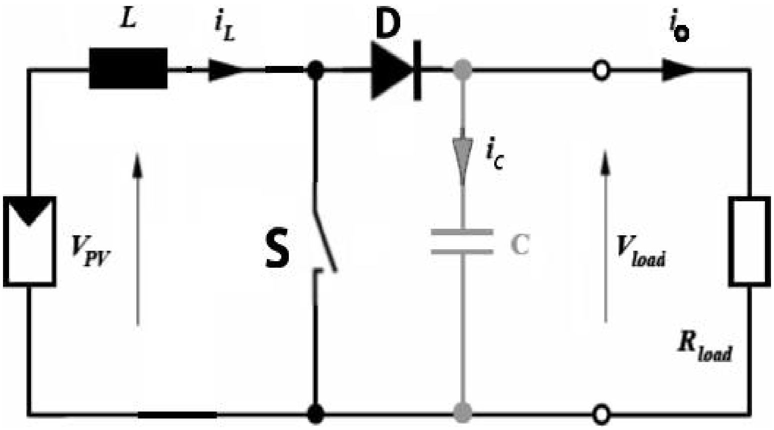

Figure 2.11. Circuit diagram of boost converter

There are two modes of operation of a boost converter. Those are based on closing and opening of the switch S. The first mode (OFF state) is when the switch S is open and it is known as the discharging mode of operation. The second mode (ON state) is when the switch S is closed also known as the charging mode of operation [24].

(a) OFF STATE:

In the OFF state, the switch S is open and the circuit becomes as shown in the Figure 2.12. The capacitor will be charged and the input current will be divided into two parts; output current i_o passes in the load resistance R and capacitor current i_c passes in the capacitor C. The duration time of switch off as well as the output voltage depend on duty ratio D according to the equations below.

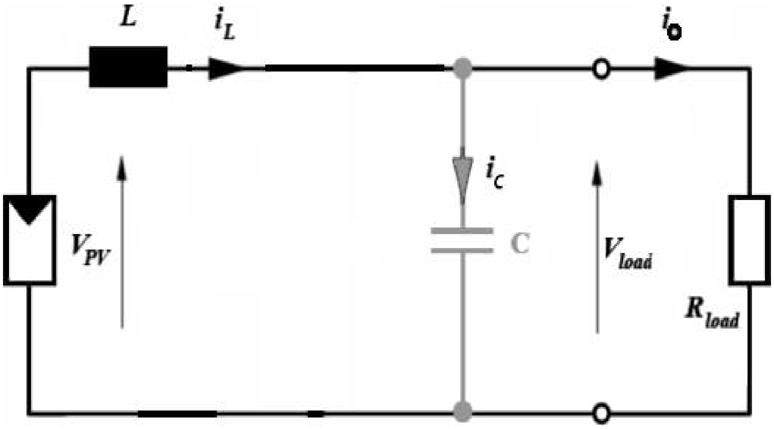

Figure 2.12. The OFF state diagram of the boost converter

(b) ON STATE:

In the ON state, the switch S is closed and the circuit becomes as shown in Figure 2.13. The inductor L is charged from the input voltage source Vpv and the capacitor C discharges across the load.

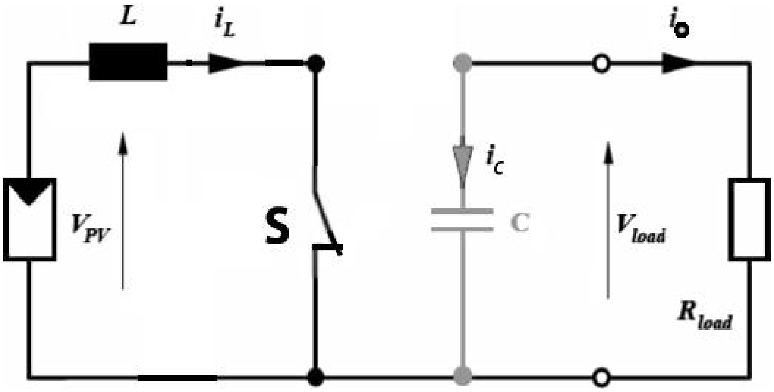

Figure 2.13. The ON state diagram of the boost converter

Assuming that all the components of the circuit are ideal, the inductor current i_L is continuous (always positive) and the output voltage is held constant at V_{load} by the large output capacitor C during the switching intervals. The following equations then hold for the boost converter:

$$\mathrm{V}_{load} = \frac{\mathrm{V}_{pv}}{1 - D} \tag{2.5}$$

$$\mathrm{I}_{max} = \frac{\mathrm{V}_{load}}{(1 - D)^2 \times \mathrm{R}_{load}} + \frac{\mathrm{V}_{load} \times D}{2 \times L \times f} \tag{2.6}$$

$$\mathrm{I}_{min} = \frac{\mathrm{V}_{load}}{(1 - D)^2 \times \mathrm{R}_{load}} - \frac{\mathrm{V}_{load} \times D}{2 \times L \times f} \tag{2.7}$$

$$I_{avg} = \frac{V_{load}}{(1 - D)^2 \times R_{load}} \tag{2.8}$$

$$Io = \frac{V_{load}}{R_{load}} \tag{2.9}$$

$$I_{pv} = \frac{I_0}{(1-D)} \tag{2.10}$$

Where, V_{load} = output DC voltage (V), V_{pv} = supply DC voltage (V), D = Duty Cycle, I_0 = output DC current (A), I_{pv} = supply DC current (A), L = inductance of the inductor (mH), R_{load} = Load resistance (Ω).

For a given switching frequency, the minimum inductance L_{min} for continuous conduction is given by:

$$L_{min} = \frac{D \times (1-D)^2 \times R_{load}}{2 \times f} \tag{2.11}$$

The current delivered to the output RC circuit is not continuous. Therefore, a large filter capacitor is necessary to minimize the voltage ripple at the output. This filter capacitor supplies the DC current to the load when the diode (D) is turned off.

The minimum value of the filter capacitance that results in the voltage ripple ΔV_{load} is given by [25] :

$$C_{min} = \frac{D \times V_{load}}{\Delta V_{load} \times R_{load} \times f} \tag{2.12}$$

During continuous mode of a boost converter, the current i_L through the inductor never drops to zero. Figure 2.14 indicates a few wave forms when the switch T is turned ON and OFF at frequency f, with a duty cycle D during continuous conduction mode:

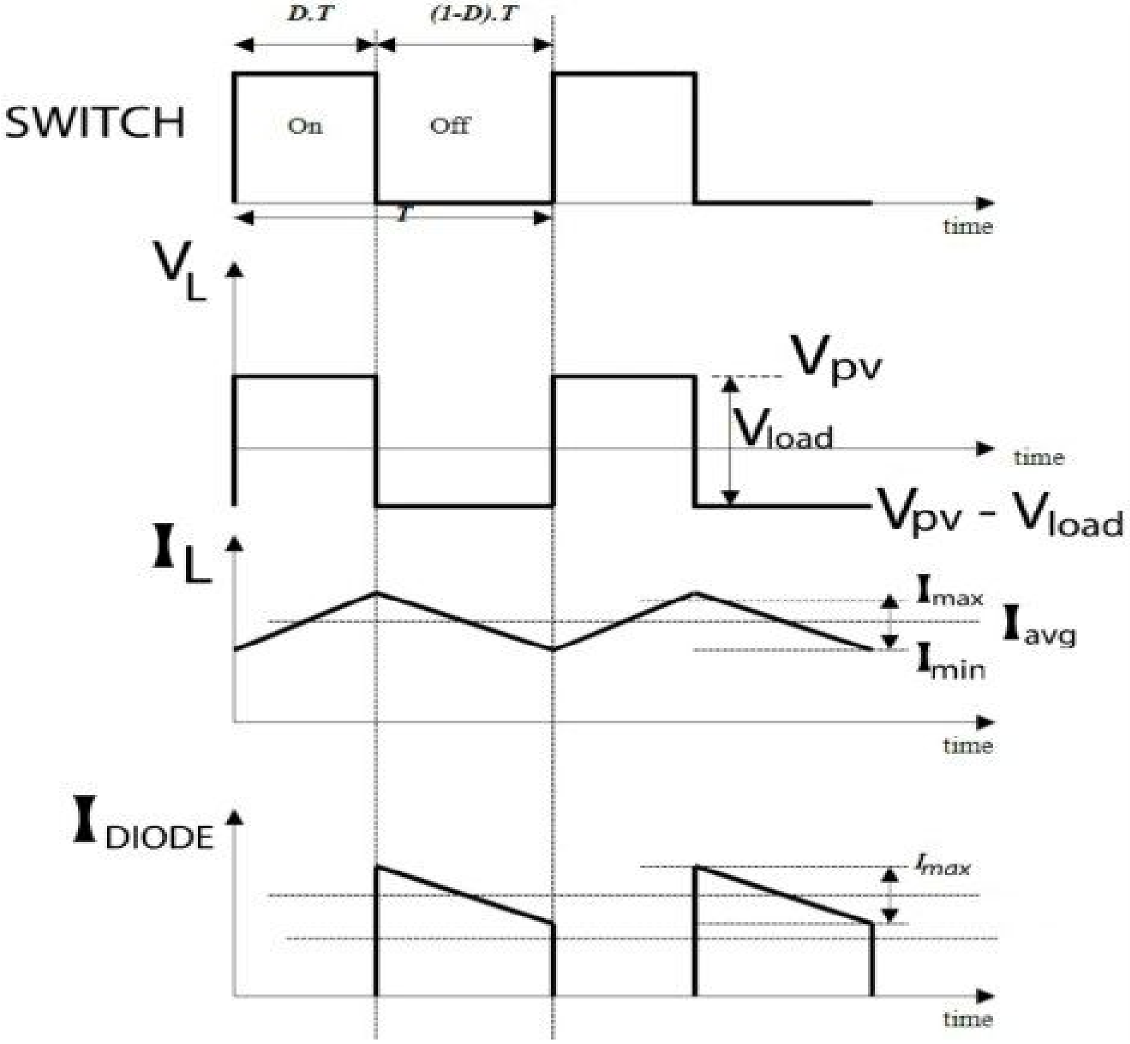

Figure 2.14. Waveforms of current and voltage in a boost converter operating in continuous mode

2.4 Three-phase VSI Inverter

Inverters play an important role in modern electrical engineering, notably in applications requiring the conversion of direct current (DC) into alternating current (AC) with three-phase outputs. These devices are crucial to different areas, including renewable energy systems, industrial motor drives, and power supply systems.

A three-phase inverter consists of six power switches labeled S1 through S6. Each switch can be in one of two states: a logical ’1’ indicates that the switch is turned on, while a logical ’0’ signifies that the switch is turned off. Each phase leg is connected to two switches such that when the upper switch (associated with S1, S3, or S5) is turned ON (set to 1), its corresponding lower switch (S4, S6 or S2) is turned OFF (set to 0)[30]. The examination of the ON/OFF states of the upper switches S1, S2 and S3 is necessary for managing the power flow to the three-phase BLDC motor.

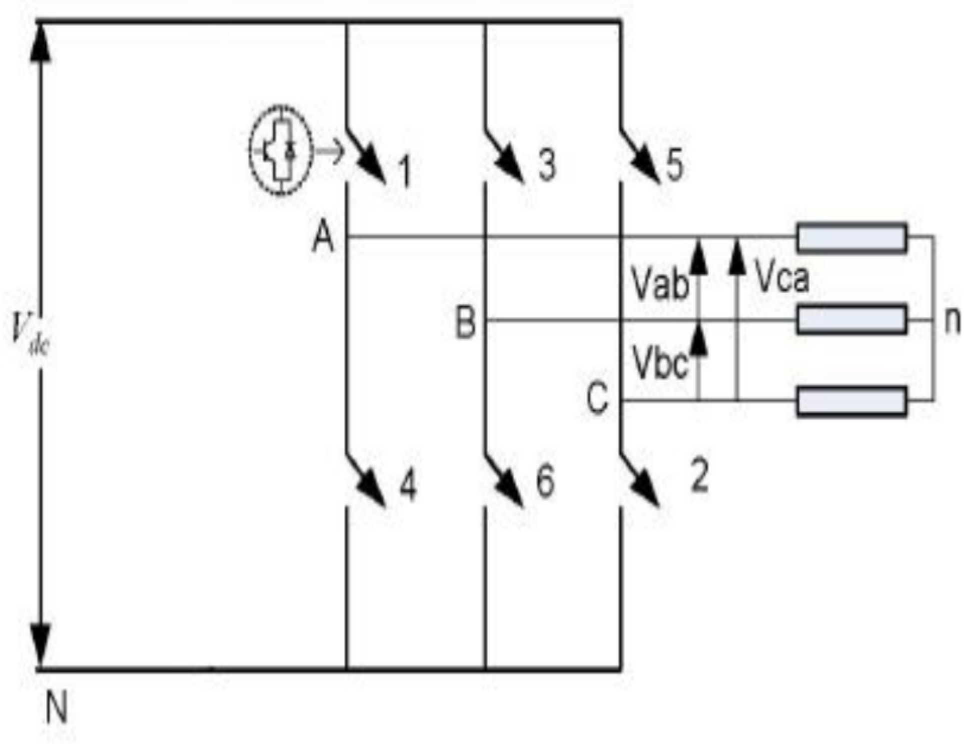

Figure 2.15. Basic circuit of three phase inverter

The relationship between the switching variable vector $[S1\ \ S3\ \ S5]^t$ and the line-to-line voltage vector $[V_{ab}\ \ V_{bc}\ \ V_{ca}]^t$ is given by (2.13) as following:

$$\begin{bmatrix} V_{ab} \\ V_{bc} \\ V_{ca} \end{bmatrix} = V_{dc} \begin{bmatrix} -1 & 1 & 0 \\ 0 & -1 & 1 \\ 1 & 0 & -1 \end{bmatrix} \begin{bmatrix} S1 \\ S3 \\ S5 \end{bmatrix} \tag{2.13}$$

Also, the relationship between the switching variable vector $[S1\ \ S3\ \ S5]^t$ and the phase voltage vector $[V_{an}\ \ V_{bn}\ \ V_{cn}]^t$ can be expressed below:

$$\begin{bmatrix} V_{an} \\ V_{bn} \\ V_{cn} \end{bmatrix} = \frac{V_{dc}}{3} \begin{bmatrix} -2 & 1 & 1 \\ 1 & -2 & -1 \\ 1 & 1 & -2 \end{bmatrix} \begin{bmatrix} S1 \\ S3 \\ S5 \end{bmatrix} \tag{2.14}$$

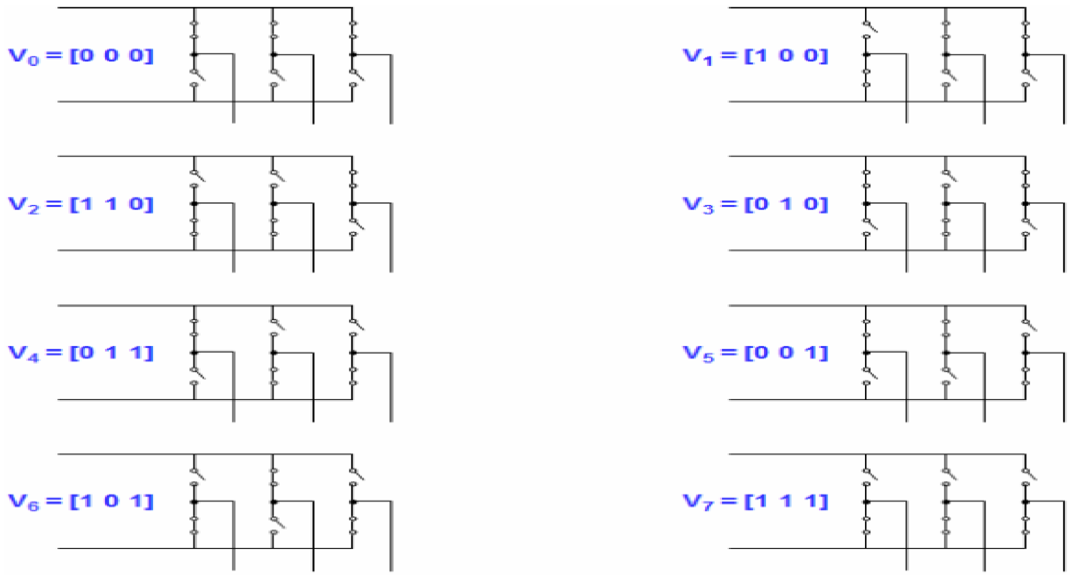

Figure 2.16. The eight inverter voltage vectors V0 to V7

Figure 2.16 illustrates that there are a total of eight potential combinations for turning the three top power switches either ON or OFF. The states of the lower power switches are just the opposite of the higher ones and can be easily determined if the states of the top switches are known.

The following Table 2.1, provides the eight switching vectors, the output phase voltages (line to neutral), and the output line-to-line voltages in terms of the DC-link voltage (Vdc), as determined by equations (2.13) and (2.14).

Table 2.1. Switching vectors, phase voltages and output line to line voltages

Voltage vectors	**Switching Vectors**			**Line to neutral voltage**			**Line to line voltage**		
	S1	**S3**	**S5**	V_{an}	V_{bn}	V_{cn}	V_{ab}	V_{bc}	V_{ca}
V0	0	0	0	0	0	0	0	0	0
V1	1	0	0	-2Vdc/3	Vdc/3	Vdc/3	-Vdc	0	Vdc
V2	1	1	0	-Vdc/3	-Vdc/3	2Vdc/3	0	-Vdc	Vdc
V3	0	1	0	Vdc/3	-2Vdc/3	Vdc/3	Vdc	-Vdc	0
V4	0	1	1	2Vdc/3	-Vdc/3	-Vdc/3	Vdc	0	-Vdc
V5	0	0	1	Vdc/3	Vdc/3	-2Vdc/3	0	Vdc	-Vdc
V6	1	0	1	-Vdc/3	2Vdc/3	-Vdc/3	-Vdc	Vdc	0
V7	1	1	1	0	0	0	0	0	0

2.5 Brushless DC Motor

2.5.1 Principle of Operation

A brushless motor is composed of a rotor that has permanent magnets and a stator with wire-wound poles. Its function is to convert electrical energy into mechanical energy by utilizing the magnetic forces between the rotor magnets and a rotating magnetic field generated in the stator poles. The fundamental principles of operation for a brushless DC (BLDC) motor are similar to those of a brushed DC motor, which involve providing feedback on the internal shaft position. However, in the case of a BLDC motor, this feedback is achieved using multiple sensors instead of a mechanical commutator and brushes. The most commonly employed sensor for this purpose is the hall senosor [26].

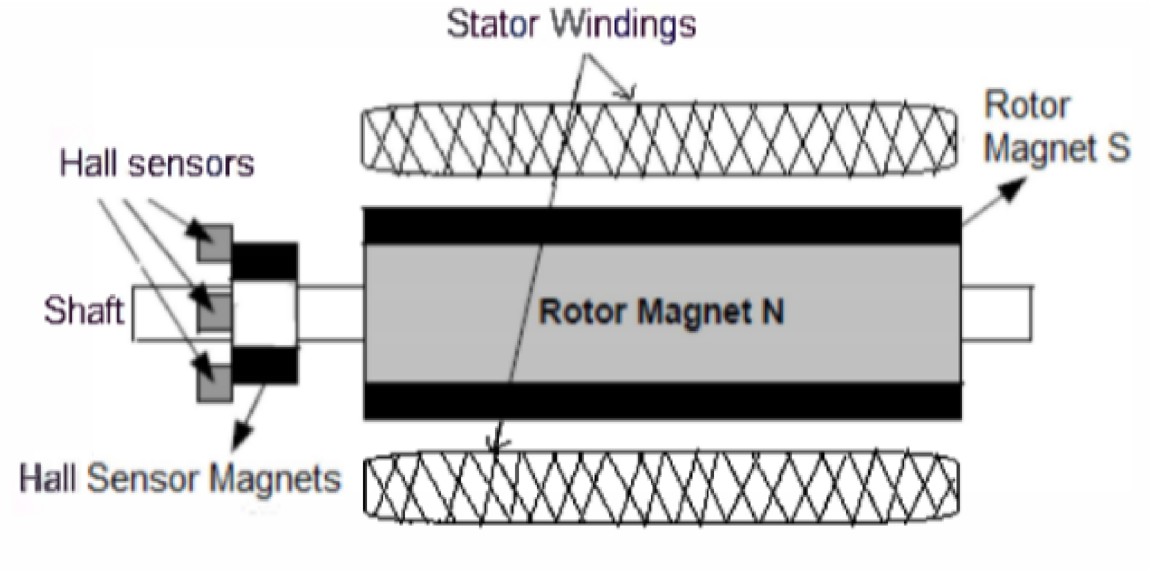

Figure 2.17. Simplified BLDC motor

2.5.1.1 Hall Effect Sensor

In contrast to a brushed DC motor, the commutation of a BLDC motor is controlled electronically. A Hall sensor is responsible for providing information to synchronize the stator armature excitation with the position of the rotor. To rotate the BLDC motor, the stator windings need to be energized in a specific sequence. Before energizing a particular stator winding, it is important to know the position of the rotor. This is where the Hall Effect sensor, embedded in the stator, comes into play by sensing the rotor position. Most BLDC motors have three Hall sensors embedded in the stator. Each sensor generates low and high signals when the rotor poles are in close proximity. By combining the responses of these three sensors, the exact commutation sequence for the stator winding can be determined [27].

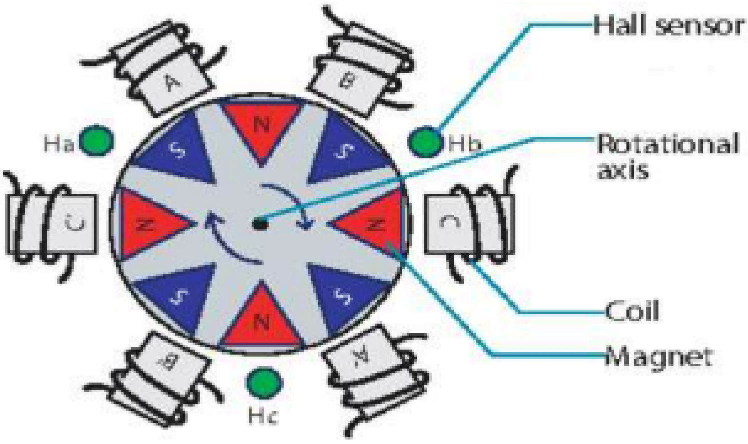

Figure 2.18. Cross section of BLDC motor

2.5.1.2 Electronic Commutation of BLDC Motor

The voltage source inverter, which controls the brushless DC motor, generates its switching signals electronically. By monitoring the position of the rotor, the hall sensors provide three hall effect signals within a 60-degree range. These hall effect signals are then converted into six switching pulses, which are used to operate the voltage source inverter.

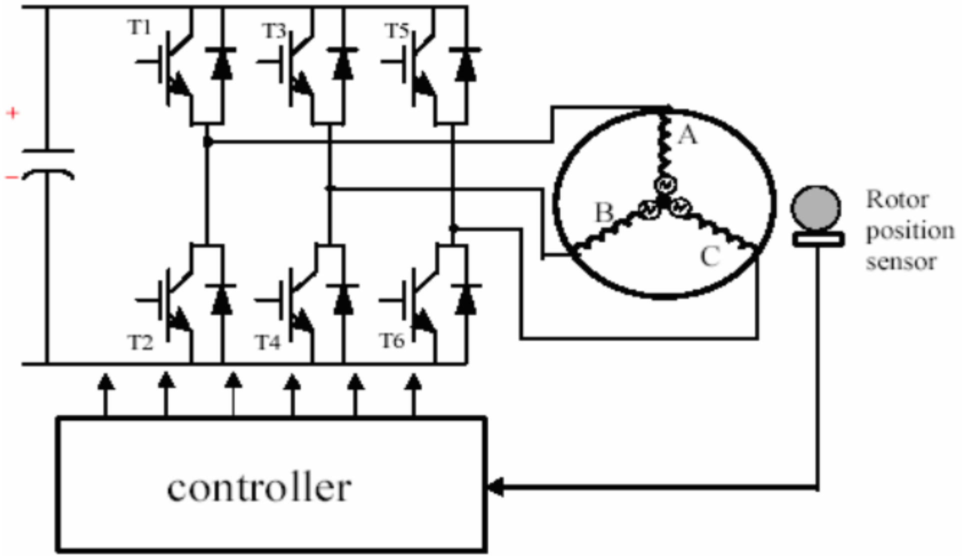

Figure 2.19. Electronic commutation of BLDC motor

The switching states of VSI for each set of Hall effect signal states is shown in the following Table 2.2.

Table 2.2. Switching states of VSI for each set of Hall-Effect signal states

Rotor Position	Hall C	Hall B	Hall A	T1	T2	T3	T4	T5	T6
NA	0	0	0	0	0	0	0	0	0
0-60	1	0	1	1	0	1	0	0	0
60-120	0	0	1	1	0	0	0	0	1
120-180	0	1	1	0	0	1	0	0	1
180-240	0	1	0	0	1	1	0	0	0
240-300	1	1	0	0	1	0	0	1	0
300-360	1	0	0	0	0	0	1	1	0
NA	0	0	0	0	0	0	0	0	0

To minimize conduction losses, only two switches are activated at any given time. As the rotor rotates, one of the Hall sensors changes its state every 60 degrees, resulting in six steps to complete an electrical cycle. In synchronous machines, the phase current switching needs to be updated every 60 electrical degrees. However, it's important to note that one electrical cycle may not align with a full mechanical rotation of the rotor. The number of electrical cycles required to complete one mechanical rotation depends on the number of rotor pole pairs.

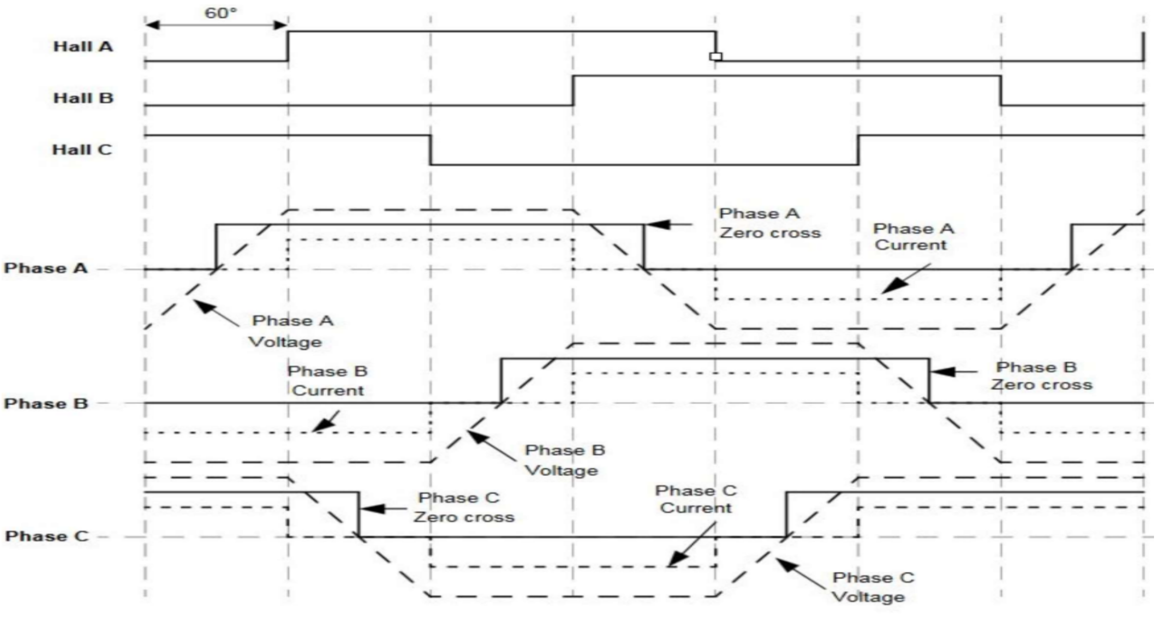

Figure 2.20. Waveform of hall sensors vs back EMF voltage

2.5.2 BLDC Dynamic Model

A brushless DC (BLDC) motor consists of three windings on the stator and a rotor equipped with permanent magnets. The inclusion of high-resistivity materials, such as stainless steel and magnets, effectively inhibits the occurrence of significant induced currents in the rotor. Our model will not consider any damper windings. By using phase variables, we can get the circuit equation for all three windings [28].

$$\begin{bmatrix} V_{as} \\ V_{bs} \\ V_{cs} \end{bmatrix} = \begin{bmatrix} R_s & 0 & 0 \\ 0 & R_s & 0 \\ 0 & 0 & R_s \end{bmatrix} + \frac{d}{dt} \begin{bmatrix} L_{aa} & L_{ab} & L_{ac} \\ L_{ba} & L_{bb} & L_{bc} \\ L_{ca} & L_{cb} & L_{cc} \end{bmatrix} \begin{bmatrix} i_a \\ i_b \\ i_c \end{bmatrix} + \begin{bmatrix} e_a \\ e_b \\ e_c \end{bmatrix} \tag{2.15}$$

where, V_{as}, V_{bs} and V_{cs} are the stator phase voltages; R_s is the stator resistance per phase; i_a, i_b and i_c are the stator phase currents; L_{aa} , L_{bb} and L_{cc} are the self-inductance of phases a, b and c; L_{ab} , L_{bc} ,and L_{ac} are the mutual inductances between phases a, b and c; e_a, e_b and e_c are the phase back electromotive forces .

It has been assumed that resistance of all the winding are equal. It also has been assumed that if there in no change in the rotor reluctance with angle because of a no salient rotor and then

$$L_{aa} = L_{bb} = L_{cc} = L \tag{2.16}$$

$$L_{ab} = L_{ba} = L_{ac} = L_{ca} = L_{bc} = L_{cb} = M \tag{2.17}$$

The stator phase currents are constrained to be balanced i.e.

$$i_a + i_b + i_c = 0 \tag{2.18}$$

This leads to the simplifications of the inductances matrix in the models as then

$$Mi_b + Mi_c = -Mi_a \tag{2.19}$$

Therefore, in state space from

$$\begin{bmatrix} V_{as} \\ V_{bs} \\ V_{cs} \end{bmatrix} = \begin{bmatrix} R_s & 0 & 0 \\ 0 & R_s & 0 \\ 0 & 0 & R_s \end{bmatrix} + \frac{d}{dt} \begin{bmatrix} L-M & 0 & 0 \\ 0 & L-M & 0 \\ 0 & 0 & L-M \end{bmatrix} \begin{bmatrix} i_a \\ i_b \\ i_c \end{bmatrix} + \begin{bmatrix} e_a \\ e_b \\ e_c \end{bmatrix} \tag{2.20}$$

It has been assume that back EMF e_a, e_b and e_c have trapezoidal waveform, where they are defined as following [26]:

$$\begin{bmatrix} e_a \\ e_b \\ e_c \end{bmatrix} = K.\omega \begin{bmatrix} f(\theta) \\ f(\theta - \frac{2\pi}{3}) \\ f(\theta + \frac{2\pi}{3}) \end{bmatrix} \tag{2.21}$$

where, k is the Back EMF constant [V/rad/s]; ω is the mechanical speed of the rotor [rad/s]; θ is the electrical rotor angle.

Total torque or the electromagnetic toque can be represented the simulation of each phase. Thus, its equation can be defined [26]:

$$T_e = \frac{(e_a \times i_a) + (e_b \times i_b) + (e_c \times i_c)}{\omega} \tag{2.22}$$

The equation of the simple motion system with inertia J [$kg.m^2$]; friction coefficient B [Nms.rad^{-1}]; load torque T_L [N*m] is [26]:

$$J\frac{d\omega}{dt} + B.\omega = (T_e - T_L) \tag{2.23}$$

The electrical rotor speed and position are related by [26]:

$$\frac{d\theta}{dt} = \frac{P \times \omega}{2} \tag{2.24}$$

2.6 Centrifugal Pump

Pumps play a vital role in various industries such as power, chemical, mineral and mining, manufacturing, and heating, air conditioning, and cooling. Specifically, a centrifugal pump is a mechanical device that uses the force of centrifugal motion to convert mechanical energy into pressure energy in the fluid it handles. These pumps are known for their high efficiency and ability to move a large volume of water [29].

A dynamic pump known as a centrifugal pump is generally used in solar water pumping system (SWPS). This type of pump is utilized because its less maintenance, reliability and better adjustment to the output of PV generators. One important aspect to note is that the torque of the pump is directly related to the square of the rotor speed. This means that as the rotor speed increases, the torque produced by the pump also increases proportionally as denoted by equation (2.25) [29].

$$T_L = Kp.\Omega_r^2 \tag{2.25}$$

where K_p is the proportionality constant and it is given by [29]:

$$K_p = P_{np}/\Omega_{rn}^3 \tag{2.26}$$

The water rate and pressure of the pump are influenced by two main factors: the mechanical power available at the rotating impeller and the total head. To simplify the process of determining the pump's output parameters, we can use affinity laws. These laws only require the pump's ratings and the actual input parameters, which include the rotor speed and torque [29].

•Affinity Laws

In order for processes to function properly, certain hydraulic parameters like head and flow rate need to be met. To estimate how changes in the pump's performance curves are affected by variations in the shaft speed (N) or impeller diameter, we can use mathematical relationships known as the Affinity Laws. These laws provide a way to understand the impact of these changes on the overall pump performance.

When the impeller diameter remains constant, the Affinity Laws explain how certain factors in a pump are affected by changes in speed. According to these laws, the flow rate (Q) of the pump will increase or decrease in direct proportion to the speed. Similarly, the head (H), which refers to the pressure the pump can generate, will change in proportion to the square of the speed. Lastly, the power required (P) to operate the pump will change in proportion to the cube of the speed. These laws provide insights into how adjustments in speed can impact the pump's flow rate, head, and power requirements[29].

$$\begin{gathered}\frac{Q_1}{Q_2} = \frac{N_1}{N_2};\\ \frac{H_1}{H_2} = (\frac{N_1}{N_2})^2;\\ \frac{P_1}{P_2} = (\frac{N_1}{N_2})^3\end{gathered} \tag{2.27}$$

2.7 Conclusion

In conclusion, this chapter provided a comprehensive overview of the component models utilized in the proposed solar water pumping system based on BLDC motor. Initially, The chapter covered the path from a PV cell into a PV array, including their characteristic curves. Furthermore, the DC-DC boost converter employed in the pumping system was introduced, along with its principle of operation and waveforms. Additionally, the modeling of the brushless DC motor was also presented to enhance understanding of motor control operations. Finally, the chapter showcased the centrifugal pump model and the principles of the affinity laws.

3. Maximum Power Point Tracking

3.1 Introduction

The main issue with solar panels or photovoltaic systems is their low efficiency in converting electrical energy depending on climatic conditions [30] and environmental factors, such as solar radiation, temperature, and partial shading. For efficient operation of the PV cell under prevailing climatic conditions, an appropriate mechanism is necessary for achieving maximum power from it, which is considered maximum power point tracking (MPPT). The MPPT increases the efficiency and lifetime of the PV module.

The quality of an MPPT technique is usually evaluated by its complexity, cost, tracking speed, accuracy, and the number of sensors required for execution [31]. So far, almost all MPPT algorithms can perform well when the PV array is under uniform solar irradiance conditions.

The convergence speed of the MPPT algorithm is a critical aspect, as improving its rise time enhances system reliability, increases power extraction, and improves overall system efficiency.

In MPPT, optimization algorithms are essential under various operating conditions, they are intended to track the Maximum PowerPoint (MPP) continuously. By optimizing the PV array output power, these algorithms raise the PV system's efficiency. In this chapter, we will see different optimization algorithm including traditional one and methaheuristics.

3.2 Maximum Power Point Tracking

The Perturb and Observe (P&O) method is one of the most used control methods in MPPT controllers and is easily implemented in practice by most of the authors. This algorithm is a simple iterative technique as it does not require previous knowledge of the PV generator characteristics or the measurement of solar intensity and cell temperature.

The P&O technique relies on the trial-and-error method in searching and following the MPP. As its name implies, it is based on the system's perturbation by increasing or decreasing the DC-DC converter's duty cycle, and then observing the effect on the output power with a view to This duty cycle [32].

Generally, the module's power and voltage (P-V) characteristic is used to track the course of the operating point of the module's output power. as shown in Figure 3.1, A positive gradient (dP/dV) The actual point is located on the left side of the MPP. A negative gradient implies that the point is on the right side of the power curve. This tracking is repeated several times until the point where dP/dV is zero, which is the tracked MPP for the PV module. The number of perturbations made in one second is called the frequency of perturbation, which can also be called the frequency of the MPPT [33].

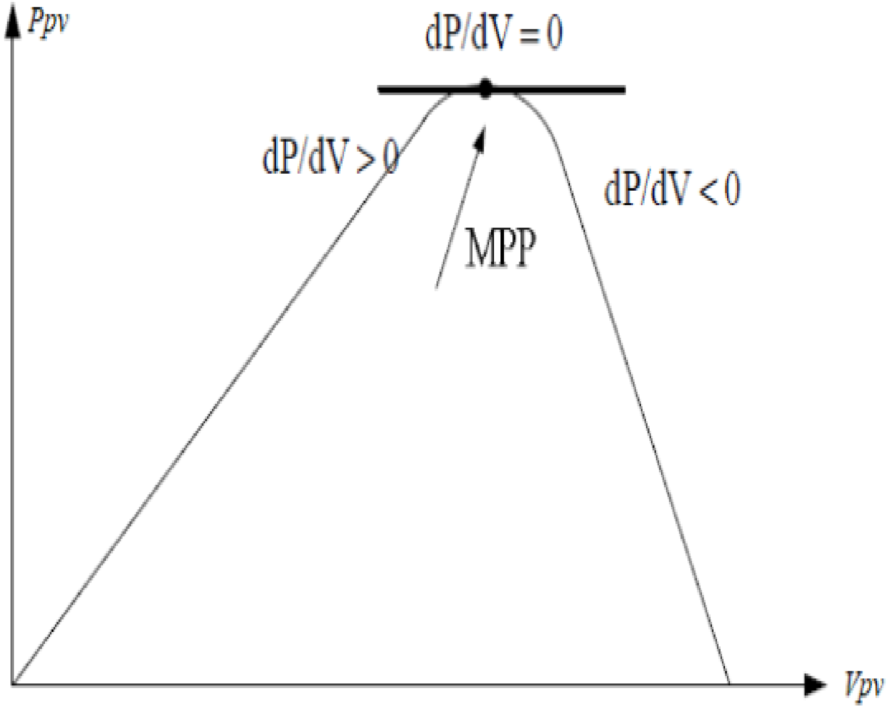

Figure 3.1. P-V characteristic of PV panel

This approach, which is the most popular algorithm, has the benefit of being straightforward to implement. The drawback of this method is that even when the maximum power is reached, energy losses from oscillations around the MPP occur, which lowers the PV system's efficiency.

Furthermore, rather than always reaching a global maximum, the control may occasionally get a local one. At the same time, this is a simple technique, and the trade-off between speed and accuracy when selecting the step size results in reduced performance.

The flowchart of the P&O algorithm is shown in the Figure 3.2 below.

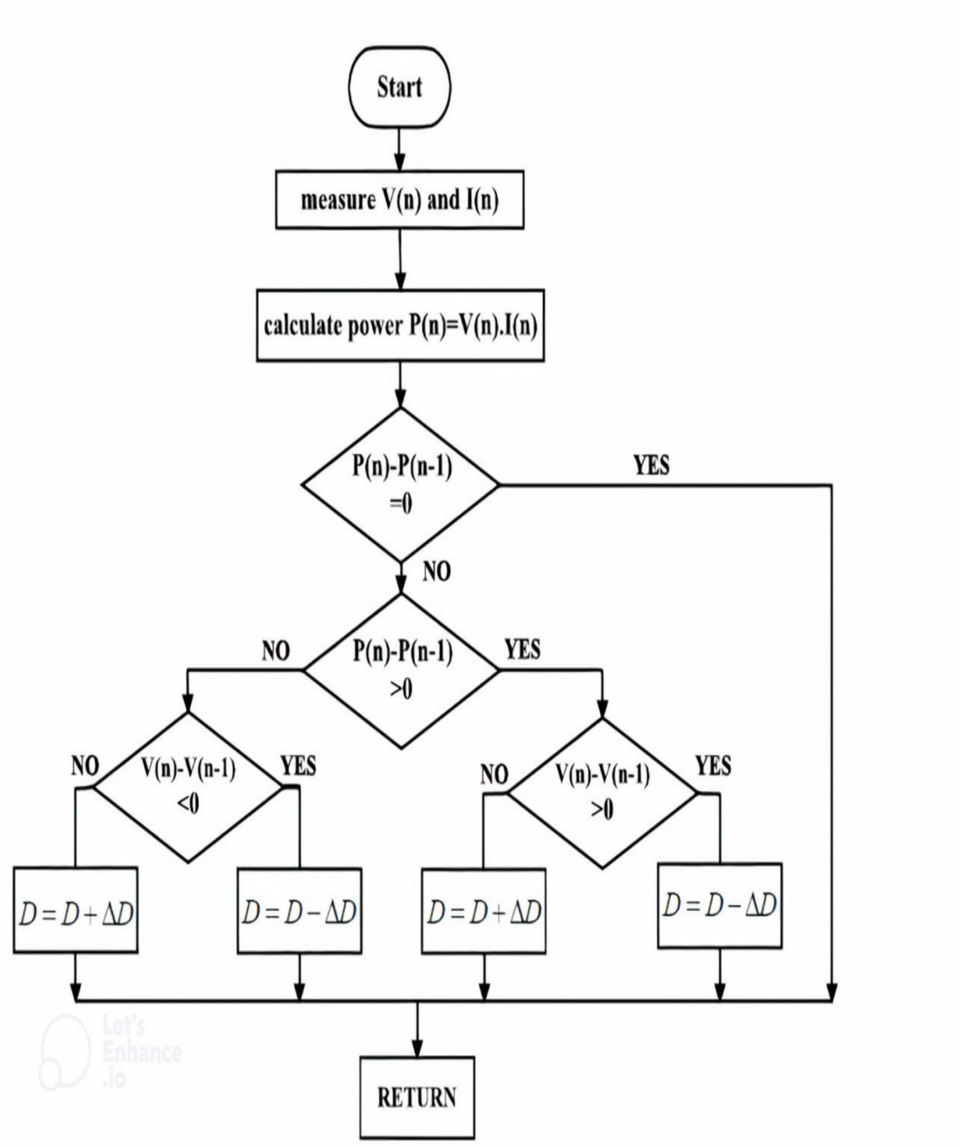

Figure 3.2. Flowchart for P&O

3.3 Partial Shading Effect

Solar panels are connected in series or parallel, depending on the required power. However, various factors such as temperature, shading, radiance, and surface angle could influence their performance.

Partial shading (PS) is the phenomenon wherein certain PV system cells or modules are partially or completely shaded as a result of aging, damage, dust, shifting clouds during the day, or nearby towers and buildings. Figure 3.3 shows the PV system and array under partial shading.

Figure 3.3. PV array under partial shading conditions

After the PV energy system is installed, a few factors might eventually arise and result in PS. The shaded PV modules negatively impact the PV system's overall efficiency and generated output power. Hot-spot and thermal breakdown issues can also arise, in which case bypass diodes must be used to protect the PV modules [34]. Rather than having a single peak under uniform conditions, P-V characteristic, under partial shading conditions (PSCs) has multiple local peaks (LPs) and one global peak (GP). It is acceptable to track the distinct MPP under uniform conditions using conventional MPPT techniques like Hill Climbing (HC), Perturb and Observe (P&O), and Incremental Conductance (IC) [35]. These techniques are also relatively easy to implement. They lack the knowledge and ability to differentiate between GP and LPs, therefore they are ineffective at tracking GP under PSCs. Furthermore, these MPPT methods may track the MPP direction incorrectly in the presence of fast fluctuations in solar irradiance [36]. PSCs or imprecise GP tracking cause incredibly high power losses in the PV system, which can surpass 70% of the total power produced. As a result, monitoring the GP is important to attain high output power, low power losses, and high power efficiency.

Researchers have proposed two efficient ways to address the problem of partial shading in photovoltaic (PV) systems. Bypass diodes are added to the PV connections in the first phase. To prevent power loss, these diodes allow current to pass around shaded cells. With the second approach, shading effects are reduced and overall performance is improved using optimization algorithms that dynamically modify the system's configuration. The effectiveness and dependability in situations with partial shading can be greatly increased by implementing either strategy.

- **Bypass diodes**

A bypass diode is a device used in solar photovoltaic (PV) arrays to protect partially shaded PV cells from fully operating cells in full sun within the same solar panel when used in high-voltage series arrays. Bypass diodes have no effect on the output of a solar cell when they are connected in reverse bias between the positive and negative output terminals [37]. By creating a current path around the problematic cell, they are used in parallel with one or more photovoltaic solar cells to stop the current from flowing from solar cells that are well-exposed to sunlight, overheating weaker or partially shaded solar cells. This is typically done because it is more economical to place bypass diodes across groups of solar cells as opposed to one per cell [37]. When a cell or panel becomes shaded or malfunctions, bypass diodes, which are wired inside the PV module, offer an alternate current. Additionally, they remove hot-spot phenomena, which can harm photovoltaic cells and potentially result in fire if light unevenly strikes the PV surface. Figure 3.4 shows the Bypass and blocking diodes in a PV system.

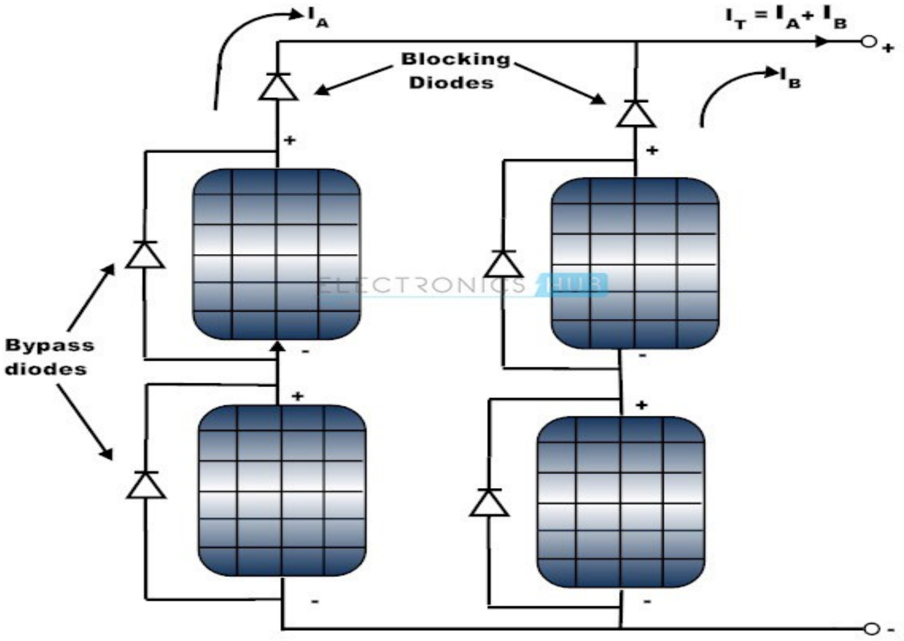

Figure 3.4. Bypass and blocking diodes in a PV system

An array with bypass diodes has different characteristics than an array without these diodes, as Figure 3.5 illustrates. When cells in a module are partially shaded, the current flowing through them changes because the bypass diodes offer an alternative current path. The power-voltage curve thus develops multiple maxima, some of which are local peaks and others of which are global maxima, or the true MPP, As a result, bypass diodes are good at turning off the hotspot and letting the PV module work reliably. However, they may have multiple MPPs on the PV characteristic when there is some shading, which can make the MPPT algorithms work less well and cause power loss [38].

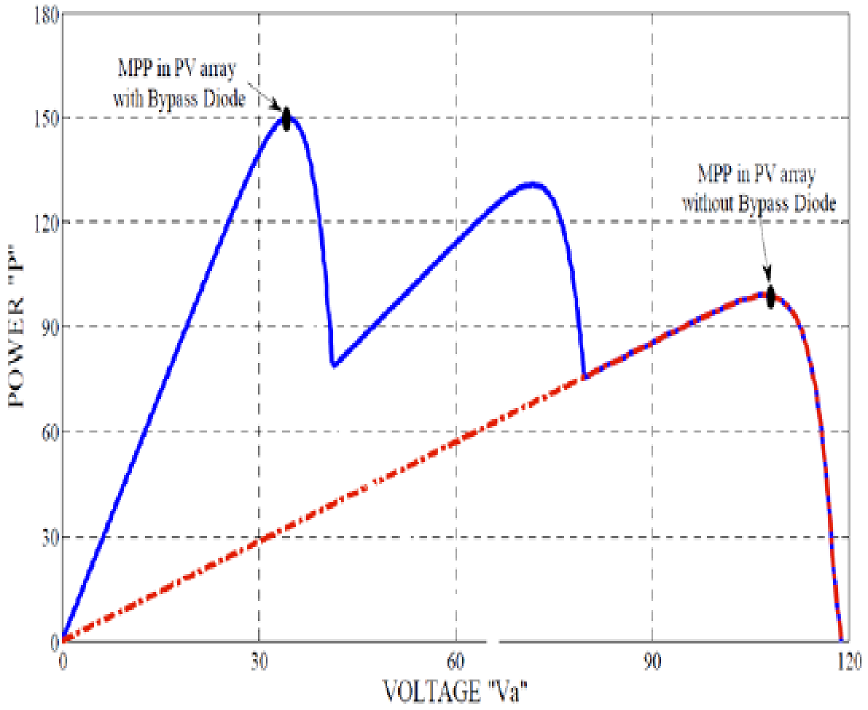

Figure 3.5. PV characteristic curves under partial shading with and without bypass diodes

3.4 Metaheuristic Algorithms

Optimization techniques known as "metaheuristic algorithms" are derived from nature or society and are applied to solve problems that are too complex for traditional algorithms or methods. Local search algorithms, global search algorithms, cooperation mechanisms between individuals, nations, states within a community, species, organisms, etc. (by this principle, these algorithms resemble life when considered as a whole), and other techniques are among them. The techniques combine to form what are known as metaheuristics, which are meant to be used for generating approximations of high-quality solutions by investigating various options. These algorithms are very flexible and robust, which makes them ideal for a wide range of real-world issues that call for intricate optimization strategies.

3.4.1 Particle Swarm Optimization (PSO)

Particle swarm optimization (PSO) is a stochastic optimization method developed by Dr. Eberhart and Dr. Kennedy in 1995 that is motivated by the social behavior of bird flocking or fish schooling and swarming theories [39]. It is a population-based search method as shown in Figure 3.6 whose purpose is to find the best possible solution to a problem, or, in other words, the minima or maxima of an objective function (in this case, the PV curve).

Figure 3.6. Birds swarm behavior

In basic terms, this algorithm makes use of the swarm intelligence concept. These bird flocks (particles) examine a particular region (search space) for food (global best). Where, they adjust their search position based on which one finds the food first. This technique is used in engineering problems where particles use the current and global best positions to update their position and velocity. The PSO is incredibly useful for solving engineering problems. Equations (3.1) and (3.2) present the PSO mathematical model.

$$V_i^{k+1} = wV_i^k + c_1 r_1 (P_{best}^k - X_i^k) + c_2 r_2 (G_{best}^k - X_i^k) \tag{3.1}$$

$$X_i^{k+1} = X_i^k + V_i^{k+1} \tag{3.2}$$

$$P_{best} = \begin{cases} P_{best} & f(X_i) \geq f(P_i) \\ X_i & f(X_i) < f(P_i) \end{cases} \tag{3.3}$$

$$G_{best} = \left\{ f(P_{best0}); f(P_{best1}); ...; f(P_{bestm}) \right\} \tag{3.4}$$

Where, m is the number of particles, k is the number of iterations, X_i and V_i are the position and velocity of particle i, w is the particle inertia weight, c_1 and c_2 are the controlling parameters, r_1 and r_2 are random numbers between 0 and 1. P_{best} and G_{best} are the personal best and global best respectively.

Each particle speed is refreshed each cycle, that consists in a set of time steps related to the number of particles used (3.1), updating the position of the group of particles at the end of the last time step (3.2) and computing a new family set of positions that will be used in the next cycle once again in (3.1).

Until the predetermined criteria are met, the final equations are applied iteratively until the convergence point is reached. Figure 3.7 displays the complete flowchart for the generic application of the particle swarm optimization algorithm.

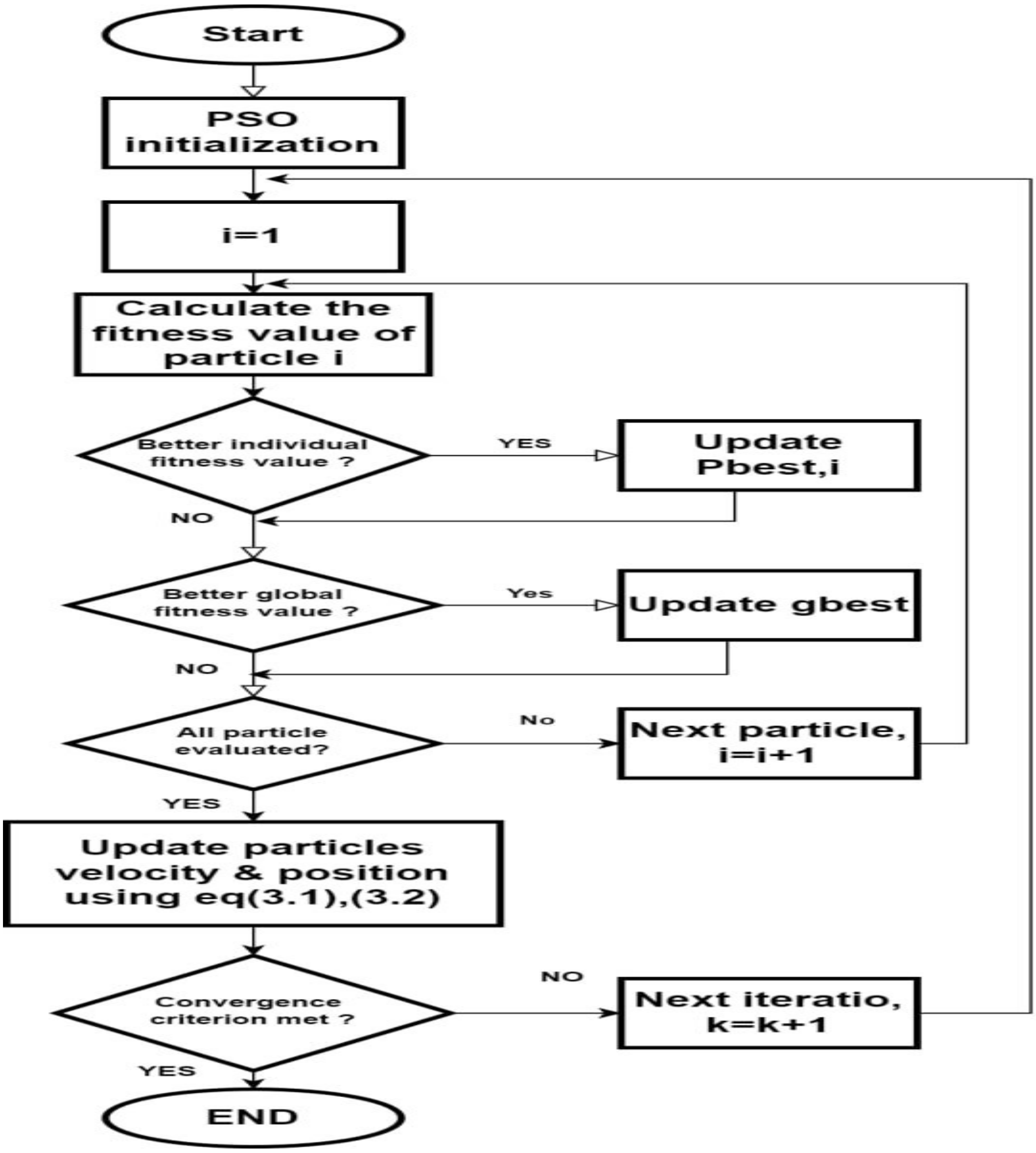

Figure 3.7. Flowchart of PSO Algorithm for MPPT Control

3.4.2 Grey Wolf Optimization (GWO)

Proposed by Mirjalili and Lewis in 2014, the GWO algorithm has been inspired by the grey wolves' hunting techniques [40]. It is considered as a meta-heuristic algorithm that illustrates the leadership hierarchy and captures grey wolves in their natural habitat while searching for potential preys.

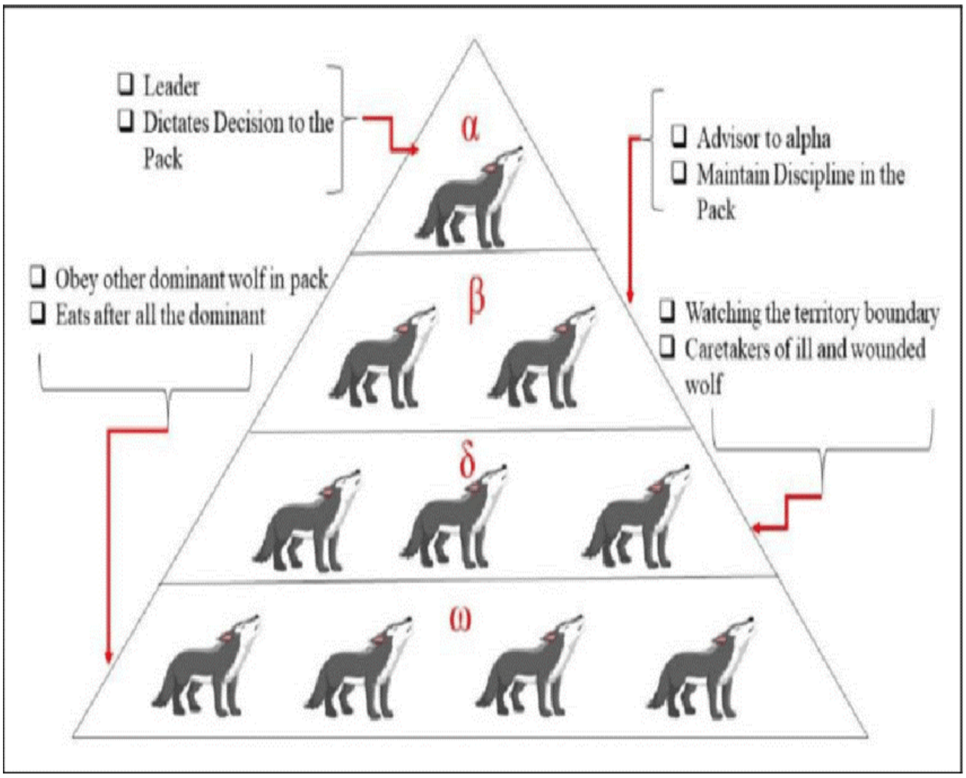

Figure 3.8. Grey wolves' hierarchy (dominance from top to bottom)

As depicted in Figure 3.8, the hierarchical structure of grey wolves, which consists of four types. The alpha wolf, the leader, makes key decisions and maintains authority through leadership rather than physical strength. The beta wolf assists the alpha in decision-making and discipline, acting as a potential successor. Next are the delta wolves, who watch the territory boundaries and care for ill or wounded pack members. At the bottom, the omega wolves act as scapegoats, submitting to all other wolves, ensuring the pack's harmony.

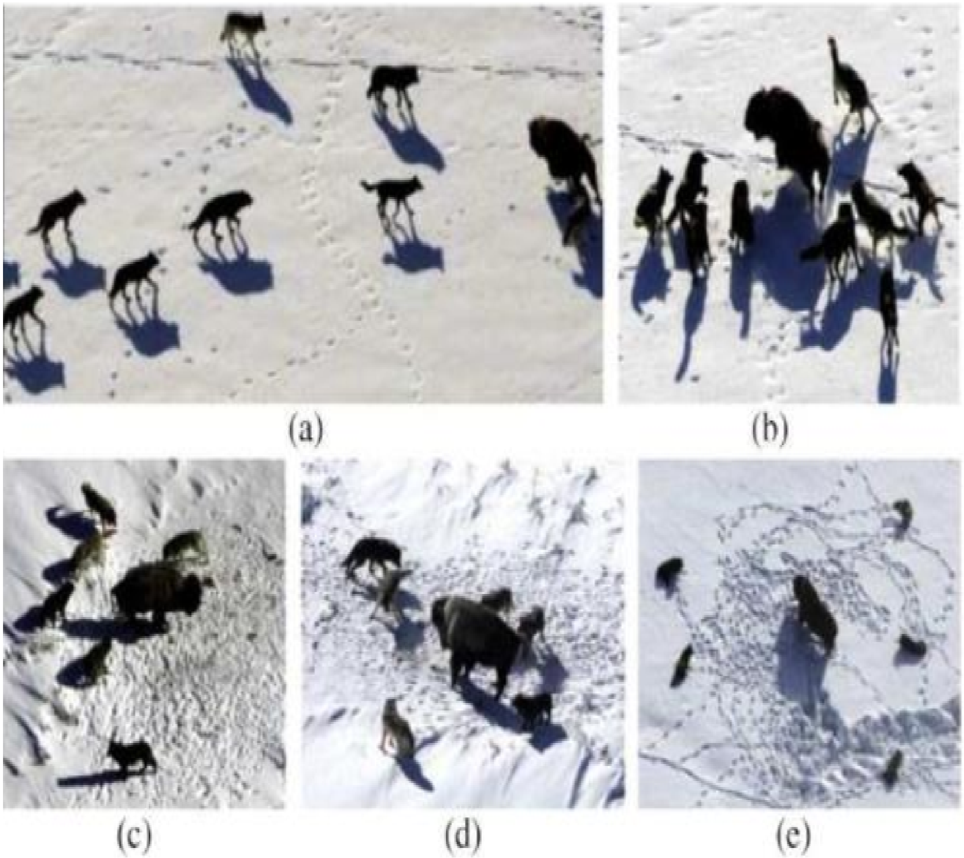

Figure 3.9. Grey wolf hunting behavior

The hunting process illustrated in the Figure 3.9 can be summurized as follows:

- Tracking, pursuing, and approaching the prey.
- Chasing, encircling, and harassing the prey until it stops moving.
- Attacking the prey.

The following equations are used to mathematically model the encircling behavior of grey wolves during a hunt:

$$\overrightarrow{V} = |\overrightarrow{C}.\overrightarrow{X_p}(t) - \overrightarrow{X_p}(t)| \tag{3.5}$$

$$\overrightarrow{X}(t+1) = \overrightarrow{X_p}(t) - \overrightarrow{A}.\overrightarrow{V} \tag{3.6}$$

Where, t denotes the current iteration. $\overrightarrow{V}$, $\overrightarrow{A}$, and $\overrightarrow{C}$ denote coefficient vectors. $\overrightarrow{X_p}$ is the position vector of the prey, and $\overrightarrow{X}$ indicates the position of grey wolf. Best solution is obtained by adjusting the coefficient vectors A and C according to Equation (3.7) and (3.8) as follows:

$$\overrightarrow{A} = \overrightarrow{a}(2\overrightarrow{r_1} - 1)) \tag{3.7}$$

$$\overrightarrow{C} = 2.\overrightarrow{r_2} \tag{3.8}$$

where, $\overrightarrow{r_1}$ and $\overrightarrow{r_2}$ are random vectors in [0,1], and component of $\overrightarrow{A}$ are linearly decreased from 2 to 0 over the course of iterations. Alpha (α), Beta (β), and Delta (δ) are more knowledgeable about the possible location of the prey during the hunt. As a result, the other search agents (omegas) adjust their positions based on these three top agents, as depicted in Figure 3.9. The formulas are as follows:

$$\overrightarrow{D}_\alpha = |\overrightarrow{C}_1.\overrightarrow{X}_\alpha - \overrightarrow{X}|; \;\; \overrightarrow{D}_\beta = |\overrightarrow{C}_2.\overrightarrow{X}_\beta - \overrightarrow{X}|; \;\; \overrightarrow{D}_\delta = |\overrightarrow{C}_3.\overrightarrow{X}_\delta - \overrightarrow{X}| \tag{3.9}$$

$$\overrightarrow{X}_1 = \overrightarrow{X}_\alpha - \overrightarrow{A}_1.(\overrightarrow{D}_\alpha); \;\; \overrightarrow{X}_2 = \overrightarrow{X}_\beta - \overrightarrow{A}_2.(\overrightarrow{D}_\beta); \;\; \overrightarrow{X}_3 = \overrightarrow{X}_\delta - \overrightarrow{A}_3.(\overrightarrow{D}_\delta) \tag{3.10}$$

$$\overrightarrow{X}(t+1) = \frac{\overrightarrow{X}_1 + \overrightarrow{X}_2 + \overrightarrow{X}_3}{3} \tag{3.11}$$

Table 3.1. The variables of GWO

The general social varibales in GWO	**In our approach**
α	**Global peak**
β	**First local peak**
δ	**Second local peak**
ω	**The rest of the local peaks**

The updating position of each grey wolf is determined by the alpha (α), beta (β), and delta (δ) values, as it is achieved by averaging or assigning the same weight to one-third of each of the three agents [35], as shown in equation (3.11). Furthermore, the Figure 3.10 displays the complete flowchart for the generic application of the grey wolf optimization algorithm.

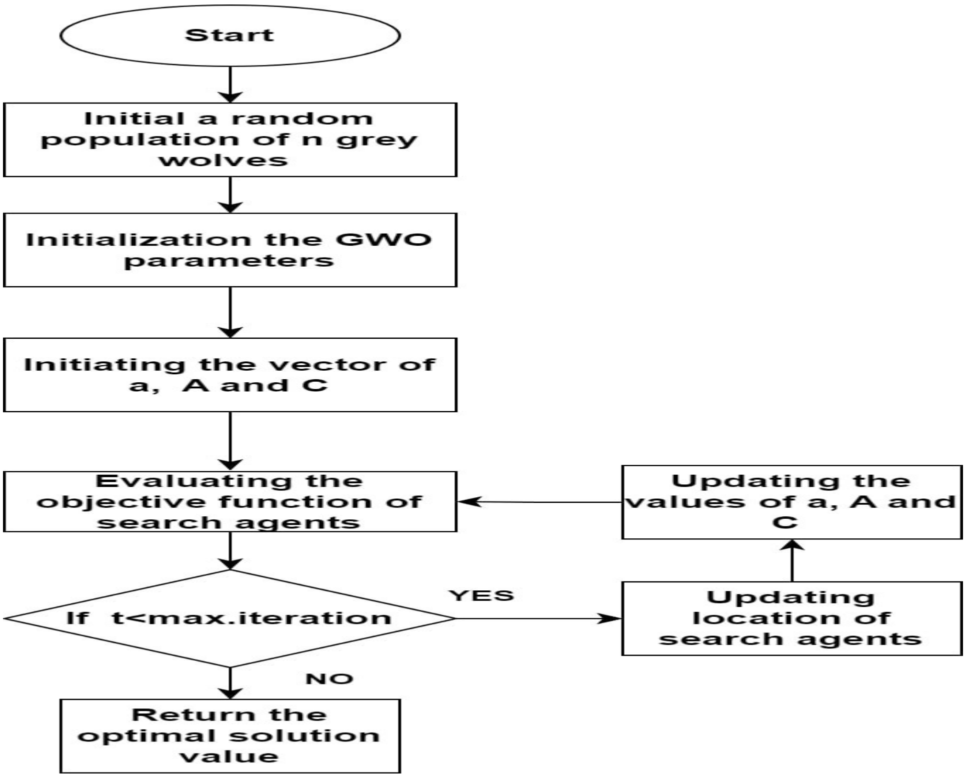

Figure 3.10. Flowchart of GWO Algorithm for MPPT Control

3.4.3 Marine Predator Algorithm (MPA)

The marine predator algorithm (MPA) is a meta-heuristic optimization that draws inspiration from nature [41]. It has been useful in solving a range of optimization issues. These issues stem from the Lévy and Brownian movements of foraging that are observed in ocean predators, as Figure 3.11 illustrates. Because of these unique features, the marine predator's technique is more complex and sophisticated than other bio-inspired methods.

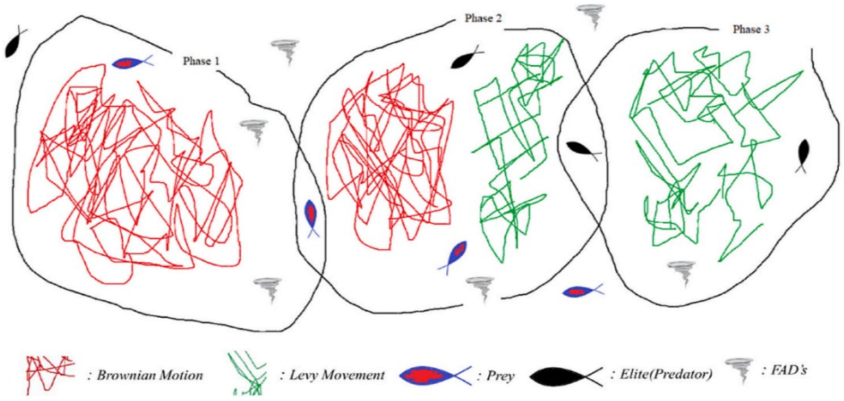

Figure 3.11. Three phases of marine predator algorithm (MPA) optimization

Marine predators are endowed with unique abilities that help them hunt in ways that are not common in other organisms. Levy motion is used in order to search over larger patches of patches at low-prey densities. In places with many prey items per unit area, however, Brownian motion enables a marine predator to exploit abundant food resources by moving randomly [41].

Additionally, marine predators possess an extraordinary memory for recognizing members of their species hence they can be able to move back together with their own kind. These mechanisms are employed to enhance this set, transforming it from a state of randomness to one in which the solutions are approximations of the global optimum of the given problem [41].

Lévy strategy is a widespread pattern among marine predators (e.g. sharks, tunas, marlines) when searching for food in a prey-sparse environment, but when it comes to foraging in a prey-abundant area, the pattern is prevalently switched to Brownian motion [42]. These strategies are mathematically described by the following equations:

$$Levy(\alpha) = 0.05 \times \frac{x}{|y|^{1/\alpha}} \tag{3.12}$$

$$f(x;\mu,\sigma) = \frac{1}{\sqrt{2\pi}} e^{\frac{-x^2}{2}} \tag{3.13}$$

Similar to other metaheuristics, MPA is also a population-based technique, It is initialized using randomly generated populations by Equation:

$$D_0 = D_{min} + rand(D_{max} - D_{min}) \tag{3.14}$$

where, D_{min} and D_{max} are the variable's lower and higher limits, respectively, while rand is a random integer.

Naturally, the topmost predators (denoted by de) are brilliant when hunting, and according to these facts An elite matrix is developed using equations:

$$\textbf{Elite} = \begin{pmatrix} de^I_{1,1} & \dots & de^I_{1,n} \\ \vdots & \ddots & \vdots \\ de^I_{m,1} & \dots & de^I_{m,n} \end{pmatrix} \tag{3.15}$$

When the predator is searching for prey, it's also important to remember that the prey is also searching for food. So, both the predator and the prey can be seen as search agents.

The elite matrix will be modified and a new size matrix known as the prey is created if the top predator is replaced by a superior predator [41]. As a result, the predator's position is periodically updated. The n^{th} position of the prey is indicated by $d_{m,n}$ in the prey matrix. The prey matrix is given in Equation (3.16).

$$\mathbf{Prey} = \begin{pmatrix} d_{1,1}^{I} & \dots & d_{1,n}^{I} \\ \vdots & \ddots & \vdots \\ d_{m,1}^{I} & \dots & d_{m,n}^{I} \end{pmatrix} \tag{3.16}$$

The optimization process is divided into three phases based on varying velocities and imitating the lives of predators and prey as shown in Figure 3.11.

The first phase is called high velocity, Predator moves slower than the prey. Whether the prey is following a Brownian or Lévy pattern, the best course of action for predators during this phase is to remain stationary and not move [43]. The following equations show the mathematical models for this phase:

$$\overrightarrow{stepsize_a} = \overrightarrow{R_B} \otimes (\overrightarrow{Elite_a} - \overrightarrow{R_B} \otimes \overrightarrow{Prey_a}); a = 1, ...n \tag{3.17}$$

$$\overrightarrow{Prey_a} = \overrightarrow{Prey_a} + P.\overrightarrow{R} \otimes \overrightarrow{stepsize_a} \tag{3.18}$$

where, P = 0.5, R is a vector of uniform random numbers in [0, 1], and R_B is the vector containing random numbers based on Brownian motion. This phase takes place For the first three iterations of the high exploration phase.

The second phase is known as unit velocity ratio. It appears when the prey and the predator are moving at the same speed. The critical phases of exploration and exploitation fall within this stage, which takes place in the middle of the iteration cycle. Consequently, half the population works on exploration projects, and the other half works on exploitation projects. This suggests that the prey is in charge of exploration and the predator is in charge of exploitation [41]. The mathematical modeling is presented in equations (3.19) and (3.20).

For first half

$$\overrightarrow{stepsize_a} = \overrightarrow{R_L} \otimes (\overrightarrow{Elite_a} - \overrightarrow{R_L} \otimes \overrightarrow{Prey_a}); a = 1, ...n/2 \tag{3.19}$$

$$\overrightarrow{Prey_a} = \overrightarrow{Prey_a} + P.\overrightarrow{R} \otimes \overrightarrow{stepsize_a} \tag{3.20}$$

Where, R_L is a random number based on Levy distribution. Step size in Levy distribution is small which helps in exploitation.

For the second half of the population

$$\overrightarrow{stepsize_a} = \overrightarrow{R_B} \otimes (\overrightarrow{R_B} \otimes \overrightarrow{Elite_a} - \overrightarrow{Prey_a}); a = n/2, ...n \tag{3.21}$$

$$\overrightarrow{Prey_a} = \overrightarrow{Elite_a} + P.CF \otimes \overrightarrow{stepsize_a} \tag{3.22}$$

where, $CF = (1 - \frac{Iter}{Iter_{max}})^{(2\frac{Iter}{Iter_{max}})}$ represents an adaptive parameter for step size controlling of predator

The third phase is low-velocity ratio. In this phase, the predator moves faster in comparison to the prey. In optimization, this is known as the exploitation phase [41]. Therefore, the best random walk in this phase is Levy-based. The phase is modeled as

$$\overrightarrow{stepsize_a} = \overrightarrow{R_L} \otimes (\overrightarrow{R_L} \otimes \overrightarrow{Elite_a} - \overrightarrow{Prey_a}); a = 1, ...n \tag{3.23}$$

$$\overrightarrow{Prey_a} = \overrightarrow{Elite_a} + P.CF \otimes \overrightarrow{stepsize_a} \tag{3.24}$$

Eddy formation or fish aggregating devices (FADs) effects are environmental issues that cause behavioral changes in marine predators.

$$\overrightarrow{Prey_a} = \begin{cases} \overrightarrow{Prey_a} + CF[\overrightarrow{D_{min}} + \overrightarrow{R} \otimes (\overrightarrow{D_{max}} - \overrightarrow{D_{min}})] \otimes \overrightarrow{U} & if \;\; r \leq FADs \\ \overrightarrow{Prey_a} + [FADs(1-r) + r](\overrightarrow{Prey_{r1}} - \overrightarrow{Prey_{r2}}) & if \;\; r > FADs \end{cases} \tag{3.25}$$

where, $\overrightarrow{U}$ is the binary vector, FADs = 0.2 which is the probability of FADs effect. $\overrightarrow{U}$ can be created by generating rand [0, 1] and change the elements to zero if it is less than 0.2 and changes to 1 is if it is greater than 0.2.

The flowchart in Figure 3.12 illustrates the process of MPA.

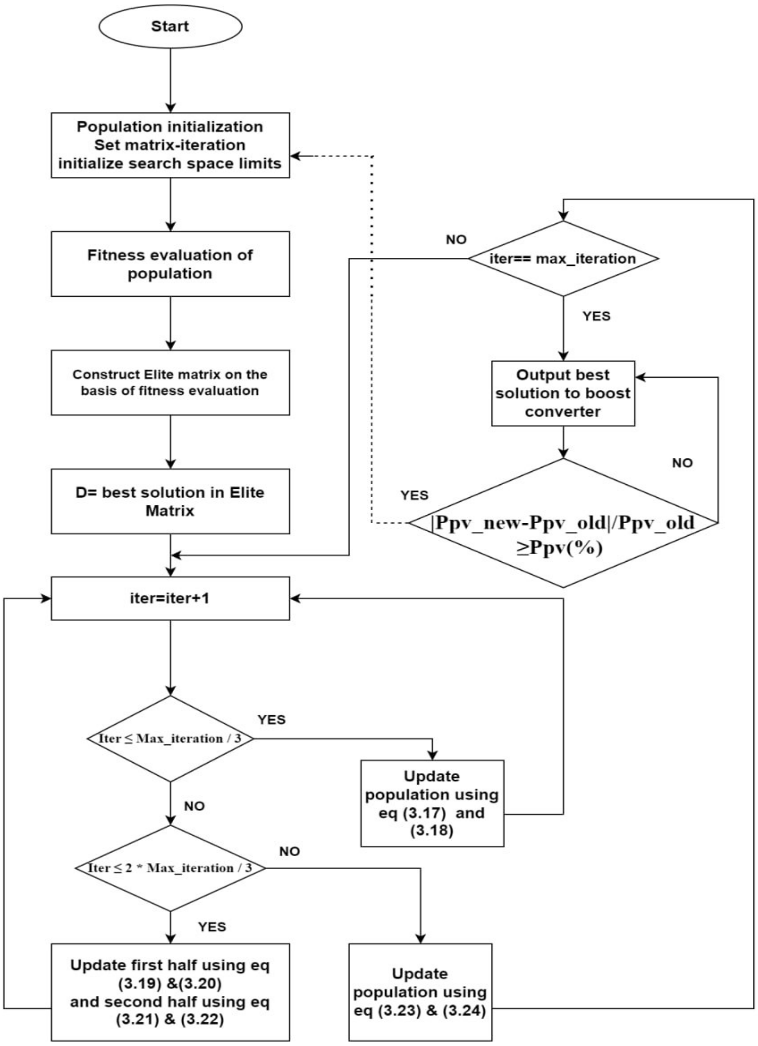

Figure 3.12. Flowchart of MPA for MPPT control

3.5 Conclusion

This chapter has given an overview about the MPPT algorithms and their importance in solar energy. Initially, we examined four commonly used techniques for tracking the global maximum power point in solar systems. These included the traditional MPPT algorithm, Perturb and Observe (P&O), which was tested under normal weather conditions with varying irradiance levels. Additionally, we presented a set of metaheuristic algorithms, Particle Swarm Optimization (PSO), Grey Wolf Optimization (GWO), and Marine Predator Algorithm (MPA), designed to handle partial shading conditions.

4. Simulation Results and Discussion

4.1 Introduction

The presented chapter demonstrates the behavior of the MATLAB/SIMULINK model of the system for solar water pumping with respect to the functioning of the solar panels and the water pump based on two cases:

- case 1: normal conditions (variable irradiance),

- case 2: partial shading conditions.

The system will be tested first to check its operation under the normal conditions (variable irradiance) and then under partial shading conditions using different optimization techniques such as Perturb and Observe (P&O), Particle Swarm Optimization (PSO), Grey Wolf Optimization (GWO), and Marine Predator Algorithm (MPA).

4.2 System Characteristics

The PV module used in the simulation is Zhejan Sunflower Light Energy Science and Technology SF125X125-72-M-175W. The detailed specifications of this module can be found in the Figure 4.1 .

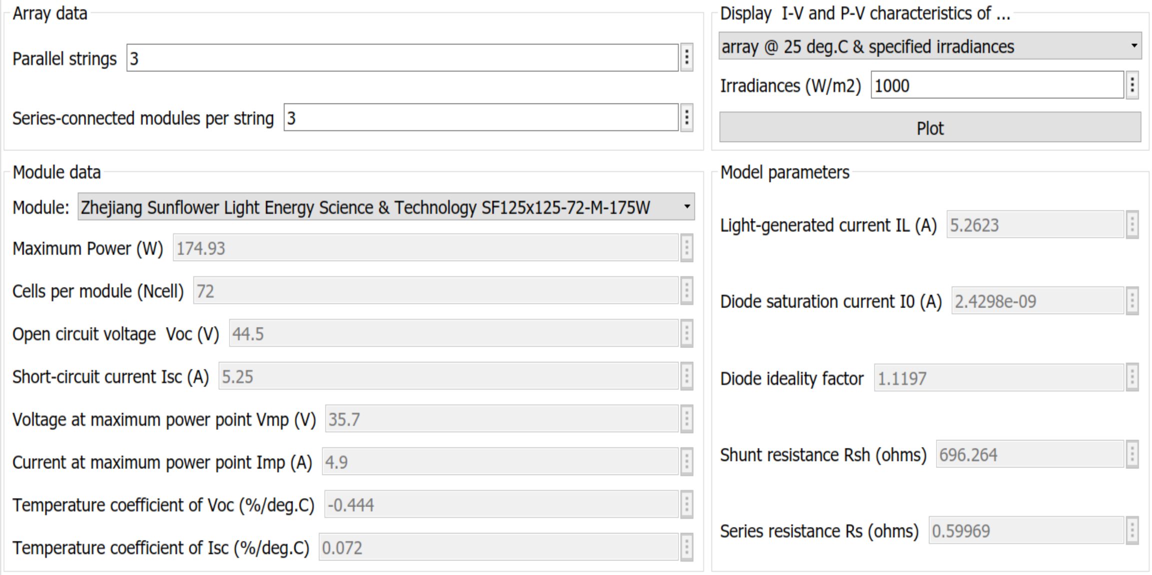

Array data
Parallel strings 3
Series-connected modules per string 3

Display I-V and P-V characteristics of ...
array @ 25 deg.C & specified irradiances
Irradiances (W/m2) 1000

Module data
Module: Zhejiang Sunflower Light Energy Science & Technology SF125x125-72-M-175W
Maximum Power (W) 174.93
Cells per module (Ncell) 72
Open circuit voltage Voc (V) 44.5
Short-circuit current Isc (A) 5.25
Voltage at maximum power point Vmp (V) 35.7
Current at maximum power point Imp (A) 4.9
Temperature coefficient of Voc (%/deg.C) -0.444
Temperature coefficient of Isc (%/deg.C) 0.072

Model parameters
Light-generated current IL (A) 5.2623
Diode saturation current I0 (A) 2.4298e-09
Diode ideality factor 1.1197
Shunt resistance Rsh (ohms) 696.264
Series resistance Rs (ohms) 0.59969

Figure 4.1. Detailed specifications of the used PV module

The system consists of a 1350 W brushless DC motor at 230 V, connected to a 1574 W PV array, having a maximum voltage of 107V and maximum current of 14.7 A. The simulation model of the used system is shown in the appendix.

4.3 Simulation of The System

As discussed in the introduction, a MATLAB/Simulink software is used to simulate the proposed water pumping system. Initially, the simulation was conducted under different cases, which included variable irradiance and partial shading. The results of the simulation for both cases are presented in the following sections.

4.3.1 Under Normal Conditions

In a normal condition, the photovoltaic (PV) array is exposed to a rapidly fluctuating, evenly distributed amount of solar radiation. This irradiance varies every second and may be categorized into three distinct levels: $1000 W/m^2$, $700 W/m^2$, and $300 W/m^2$ as shown in the Figure 4.2. Furthermore, the Figure 4.3 illustrates a graphical representation of the I-V and P-V properties of the PV array at different levels of irradiance. In order to improve the efficiency of our system under these varying irradiances, Perturb and Observe (P&O) algorithm was simulated to ensure that the maximum power is being extracted from the PV array despite the frequently changing irradiance levels.

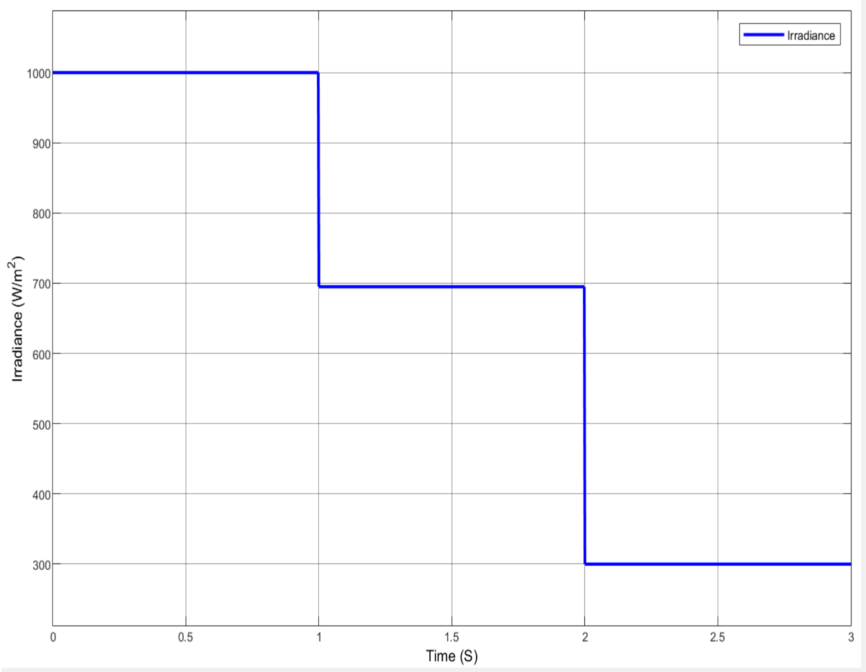

Figure 4.2. Irradiance level under normal conditions

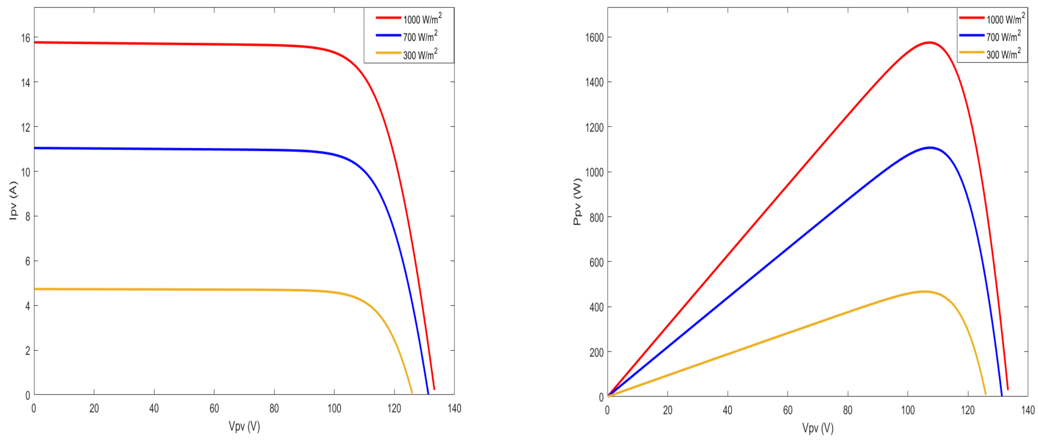

(a)

(b)

Figure 4.3. I-V and b- P-V characteristics of three PV modules in series under uniform conditions

4.3.1.1 Steady State and Starting Performances Using P&O

- **Performance of SPV Array**

The Figure 4.4 illustrates the performance of the PV power, voltage, and current using perturb and observe algorithm under variable irradiances.

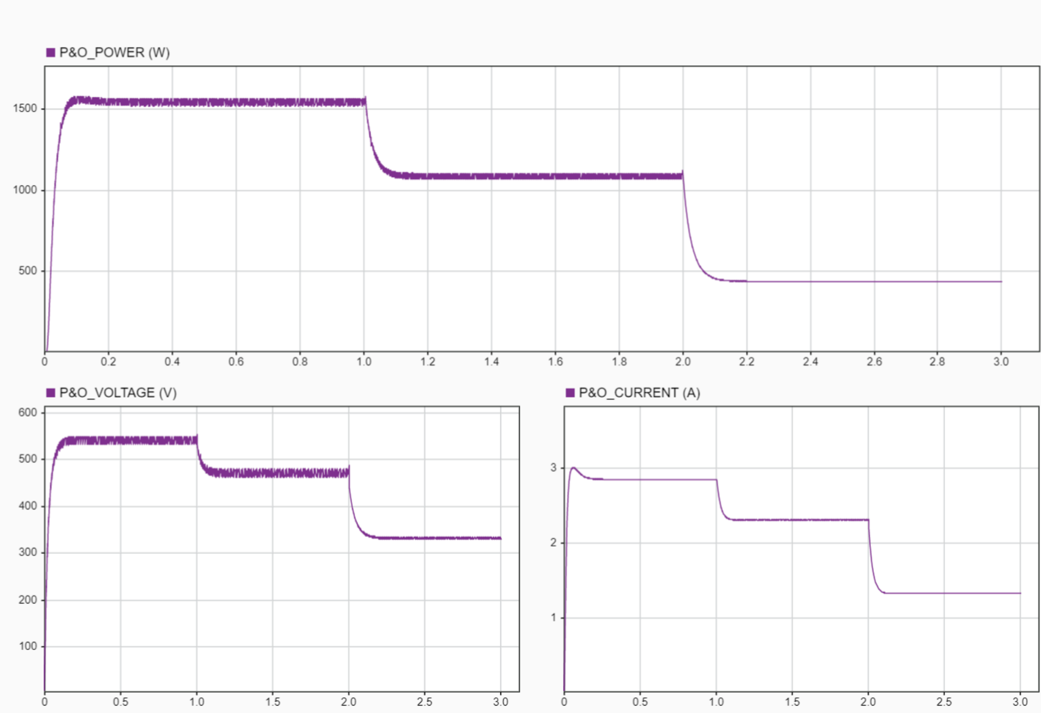

Figure 4.4. Dynamic PV performance of the proposed system using P&O algorithm under variable irradiances

The PV power, voltage, and current follow the same shape of irradiance levels curve. Initially, the power curve rapidly reaches the maximum power point despite changes in irradiance. However, in the steady-state notable noises are observed only in the power and voltage curves while the PV current remains noise-free. The remarkable noises could be attributed to increased power generation, which increases the system's sensitivity to the perturbations of the P&O algorithm. Moreover, The response and reflection speeds differ between irradiance levels, with slower convergence at lower levels.

- **Performance of Synchronous BLDC Motor Pump**

The Figure 4.5 displays the rotor speed W_m, load torque T_L, and electromagnetic torque T_e under variable irradiances using perturb and observe algorithm.

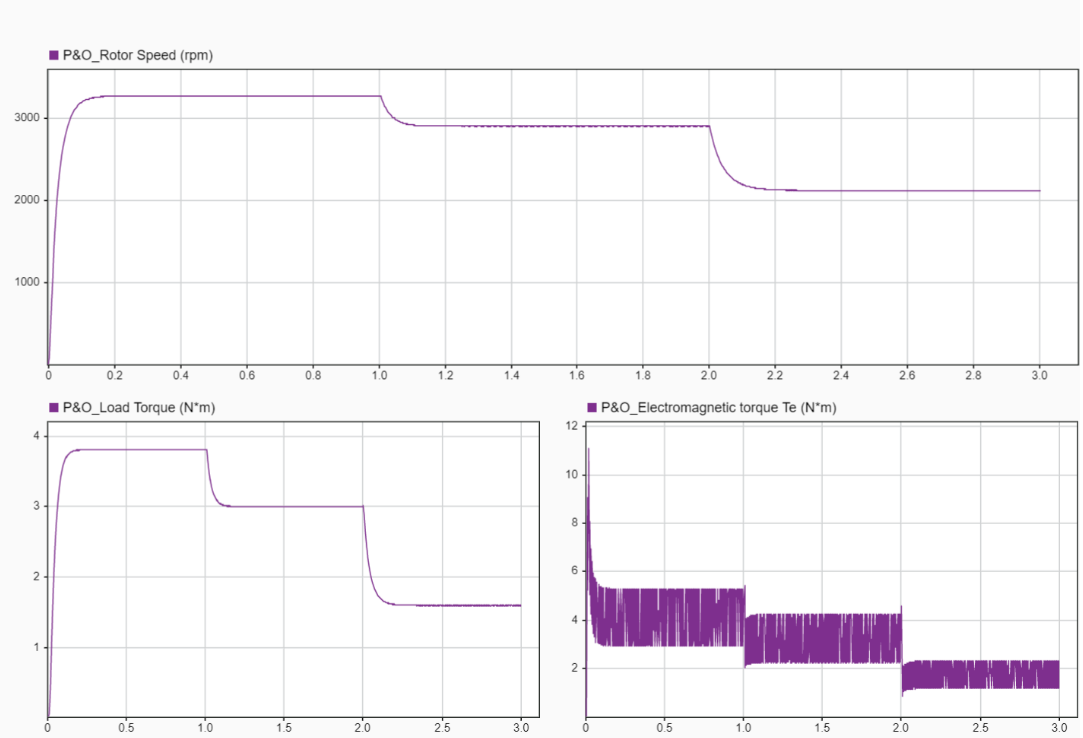

Figure 4.5. Dynamic performance of the BLDC motor of the proposed water pumping system under variable irradiances using P&O

It can be seen that the P&O algorithm provides smooth, stable-speed motor responses following the same shape of irradiance levels. This demonstrates robust performance during both transient and steady states, with noticeable speed transitions between each irradiance level. The transition from high (1000 W/m^2) to moderate (700 W/m^2) irradiance level is particularly fast compared to the transition from moderate (700 W/m^2) to low (300 W/m^2) irradiance level. Additionally, there is rapid convergence time, allowing the system to reach its optimal value in a short time. Since the load torque follows the motor speed, they exhibit similar performances, as evidenced by their similar curves. Moreover, the electromagnetic torque also follows the change in irradiance level as it depends on the PV power.

4.3.2 Under Shading Conditions

The I-V and P-V graphs illustrate the performance of a photovoltaic (PV) system under partial shading conditions with irradiance levels of 1000 (W/m^2), 700 (W/m^2), and 300 (W/m^2). The curve on the left (Figure 4.6a) shows a stepped decrease in current as voltage increases, reflecting the impact of different irradiance levels on various sections of the PV array. This non-uniform shading creates multiple local maxima in the P-V curve as seen in the multiple peaks (Figure 4.6b). The global maximum power point is at the highest peak (784 W), representing the optimal operating point for maximum power extraction.

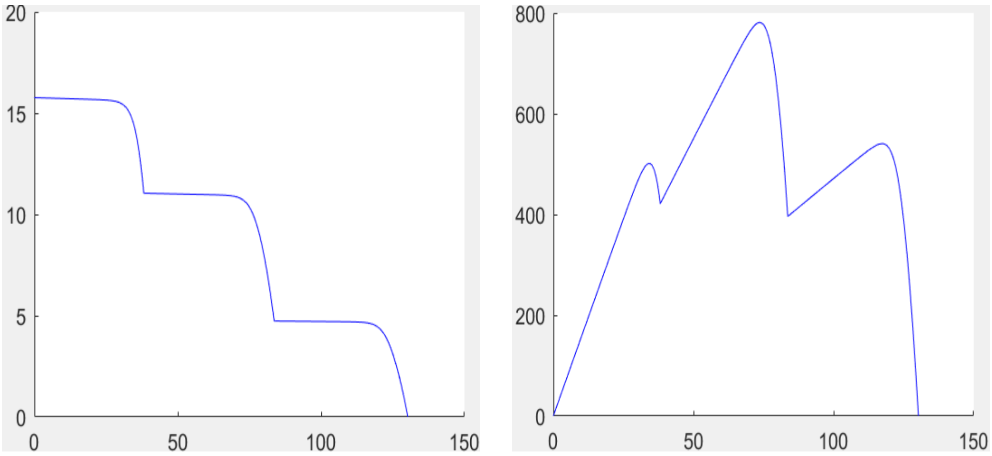

(a) (b)

Figure 4.6. (a) I-V and (b) P-V characteristics of three PV modules in series under partial shading conditions

4.3.2.1 Steady State and Starting Performances Using P&O

• Performance of SPV Array

The Figure 4.7 illustrates the performance of PV power, voltage, and current using perturb and observe algorithm under partial shading conditions.

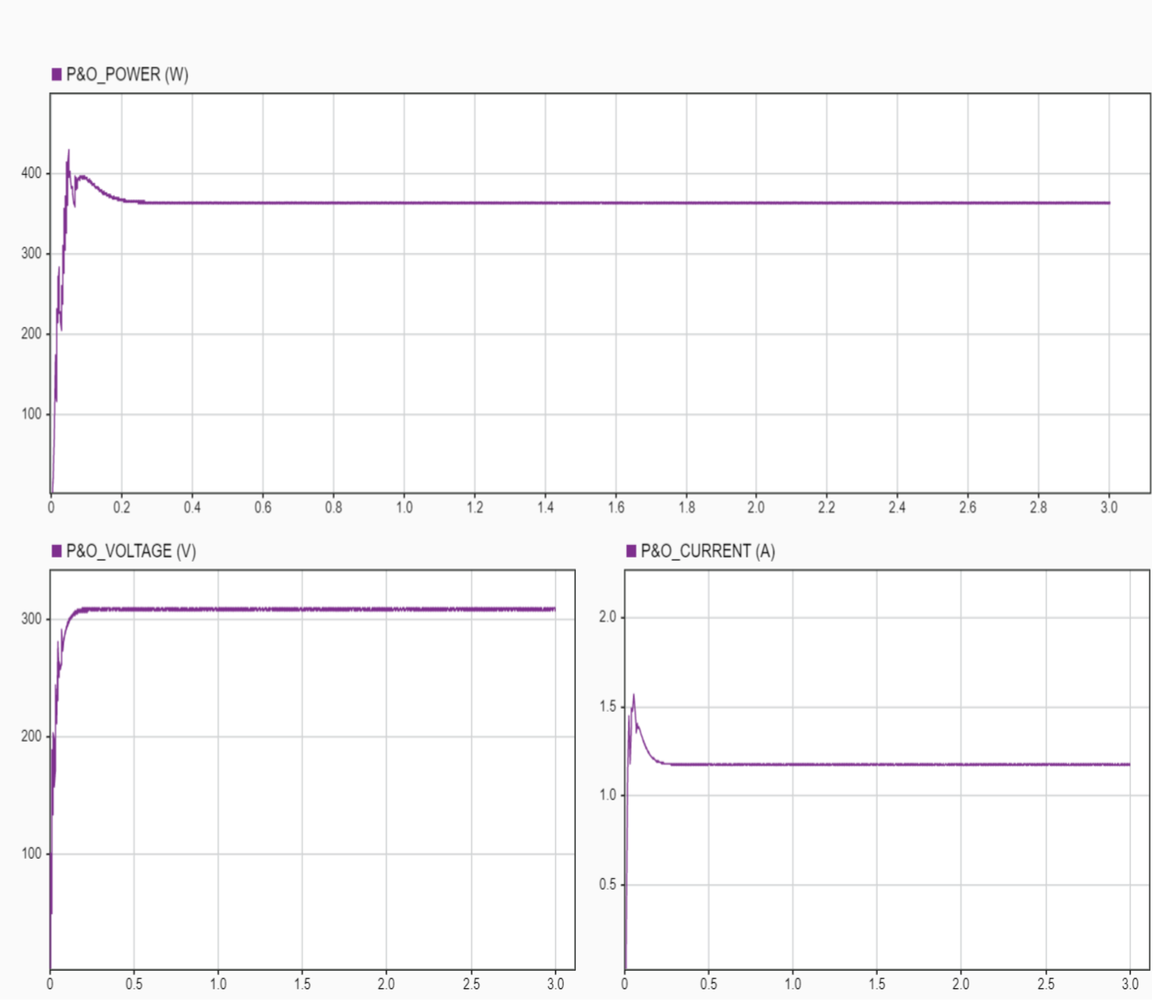

Figure 4.7. Dynamic PV performance of the proposed system under partial shading conditions using P&O algorithm

Initially, the PV power, voltage, and current exhibit significant fluctuations that can be attributed to the nature of P&O algorithm. Moreover, all the previous parameters had a fast convergence time and quickly reaching steady state at 0.5 seconds. However, it can be noticed that the power could not reach 784 W and stabilized at 363.9 W. Hence, the used P&O algorithm failed to track the global maximum power point (GMPP) and got trapped in a local maximum power point (LMPP) instead.

• Performance of BLDC Motor Pump

The Figure 4.8 displays the rotor speed W_m, load torque T_L, and electromagnetic torque T_e under variable irradiance using perturb and observe algorithm.

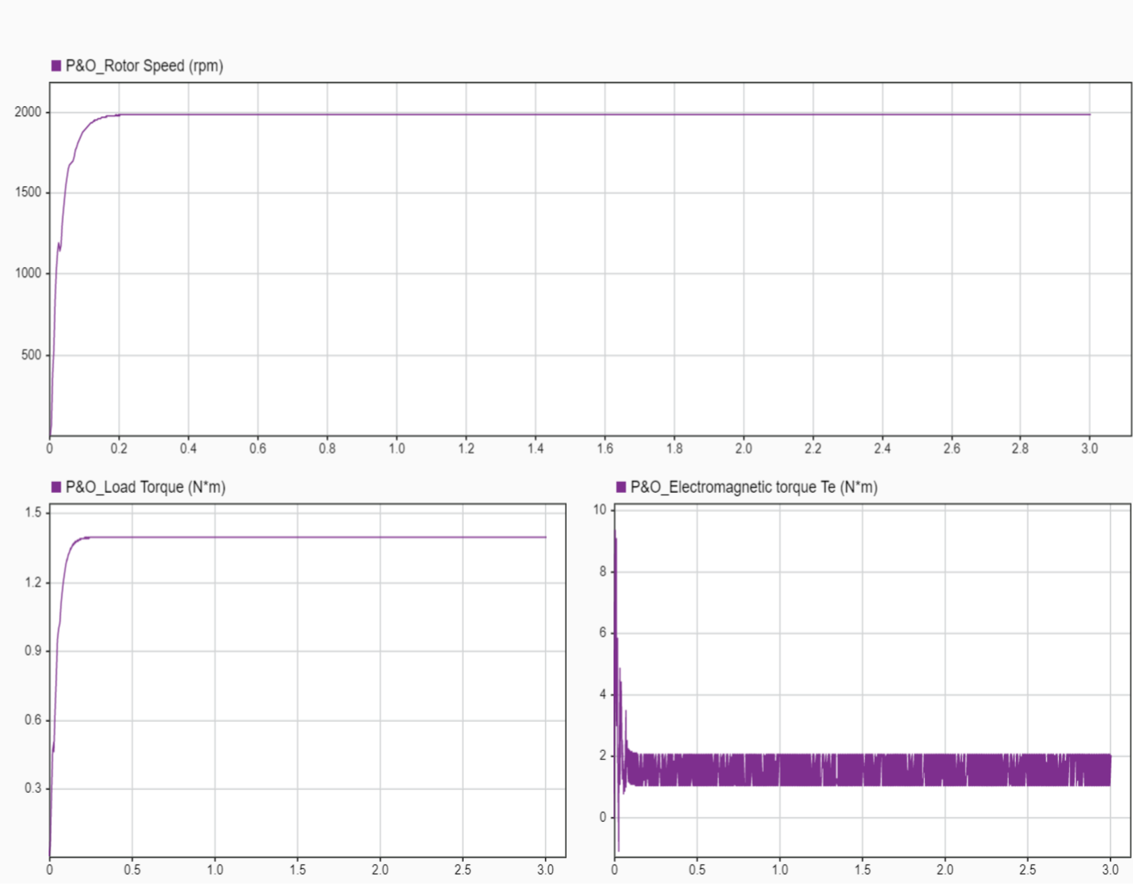

Figure 4.8. Dynamic BLDC motor performance of the proposed system under partial shading conditions using P&O algorithm

Initially, the rotor speed W_m and load torque T_L illustrate a rapid convergence time of 0.6 seconds and quickly reaching steady state with their respective values of 1987.1 rpm and 1.39 N*m. However, it can be noticed that the electromagnetic torque T_e is quite noisy at the beginning due to the motor starting, then reduces and stabilizes after a short time.

According to the steady state and starting performances using P&O, It can be noticed that the presence of multiple local maxima poses a challenge for the perturb and observe algorithm, as it failed to track the global maximum power point (784 W). This underscores the need for advanced metaheuristic algorithms that can effectively navigate these complexities to ensure efficient power extraction and reliable operation of the PV system under partial shading conditions.

4.3.2.2 Steady State and Starting Performances Using PSO

• Performance of SPV Array

The Figure 4.9 illustrates the behavior of the PV power, voltage, and current under a partial shading conditions using particle swarm optimization algorithm.

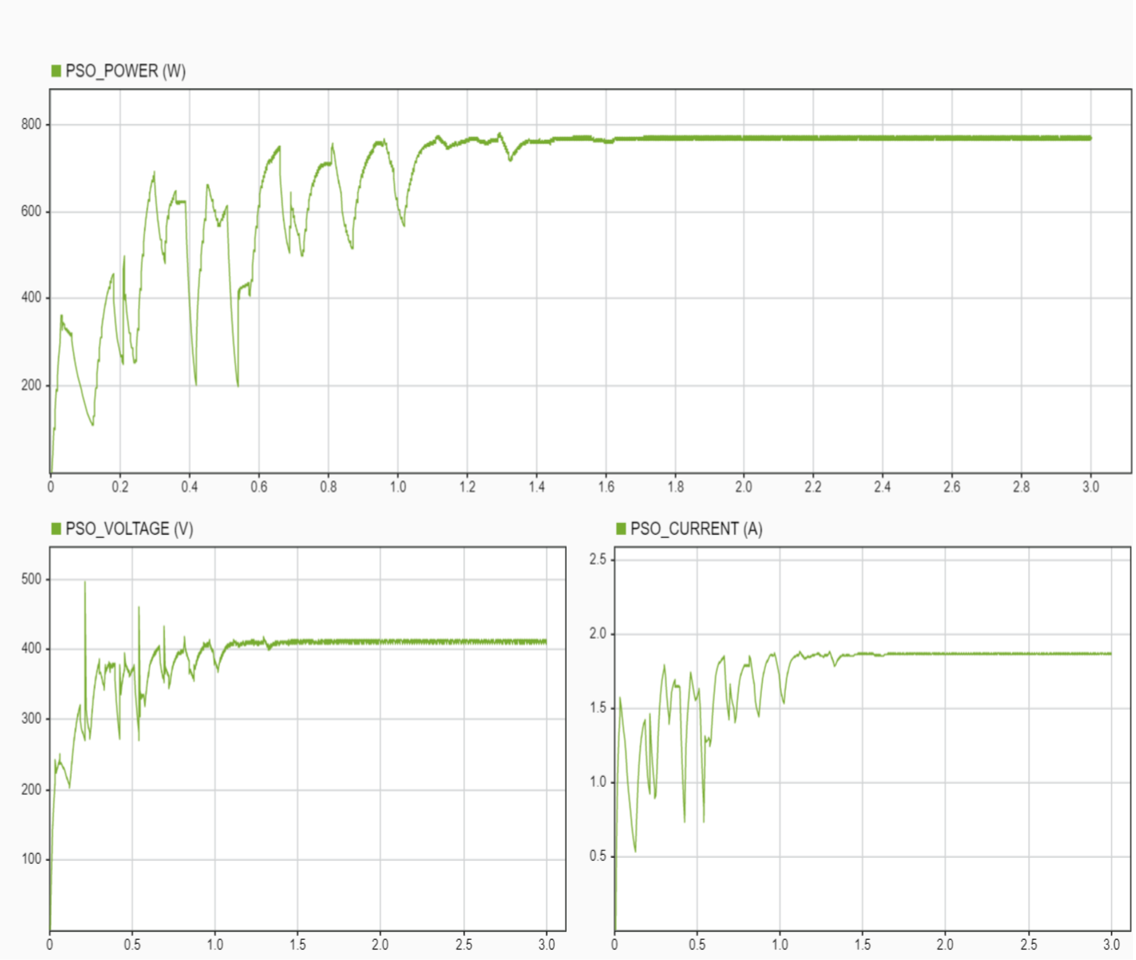

Figure 4.9. Dynamic PV performance of the proposed system under partial shading conditions using PSO algorithm

Initially, the PV power, voltage, and current curves exhibit oscillations reflecting the searching process of the PSO algorithm. However, at 1.4 seconds, the system stabilizes, and the power is 771.8 W, indicating that the PSO algorithm has successfully identified the global maximum power point (GMPP).

- **Performance of Synchronous BLDC Motor Pump**

The Figure 4.10 displays the rotor speed W_m, load torque T_L, and electromagnetic torque T_e under variable irradiance using particle swarm optimization algorithm.

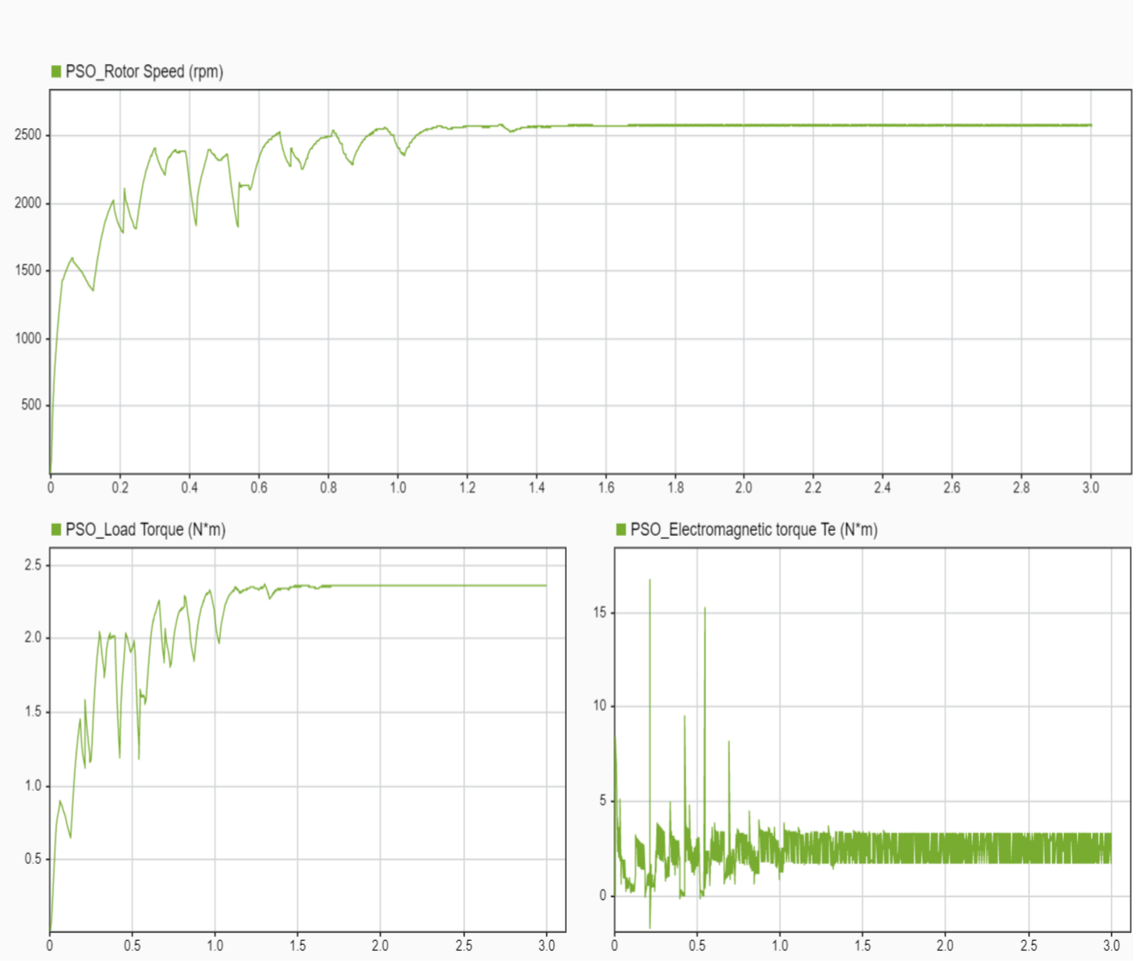

Figure 4.10. Dynamic BLDC motor performance of the proposed system under partial shading conditions using PSO algorithm

The rotor speed W_m increases rapidly with initial oscillations and stabilizes around 1.4 seconds, reaching 2588.4 rpm at steady state. The load torque T_L follows a similar pattern, rising quickly and oscillating before stabilizing at around 2.37 N*m. However, the electromagnetic torque T_e shows significant initial fluctuations, reflecting the system's efforts to reach optimal performance, and stabilizes over time, indicating reduced oscillations.

4.3.2.3 Steady State and Starting Performances Using GWO

• Performance of SPV Array

The Figure 4.11 illustrates the behavior of the PV power, voltage, and current using grey wolf optimization algorithm under partial shading conditions.

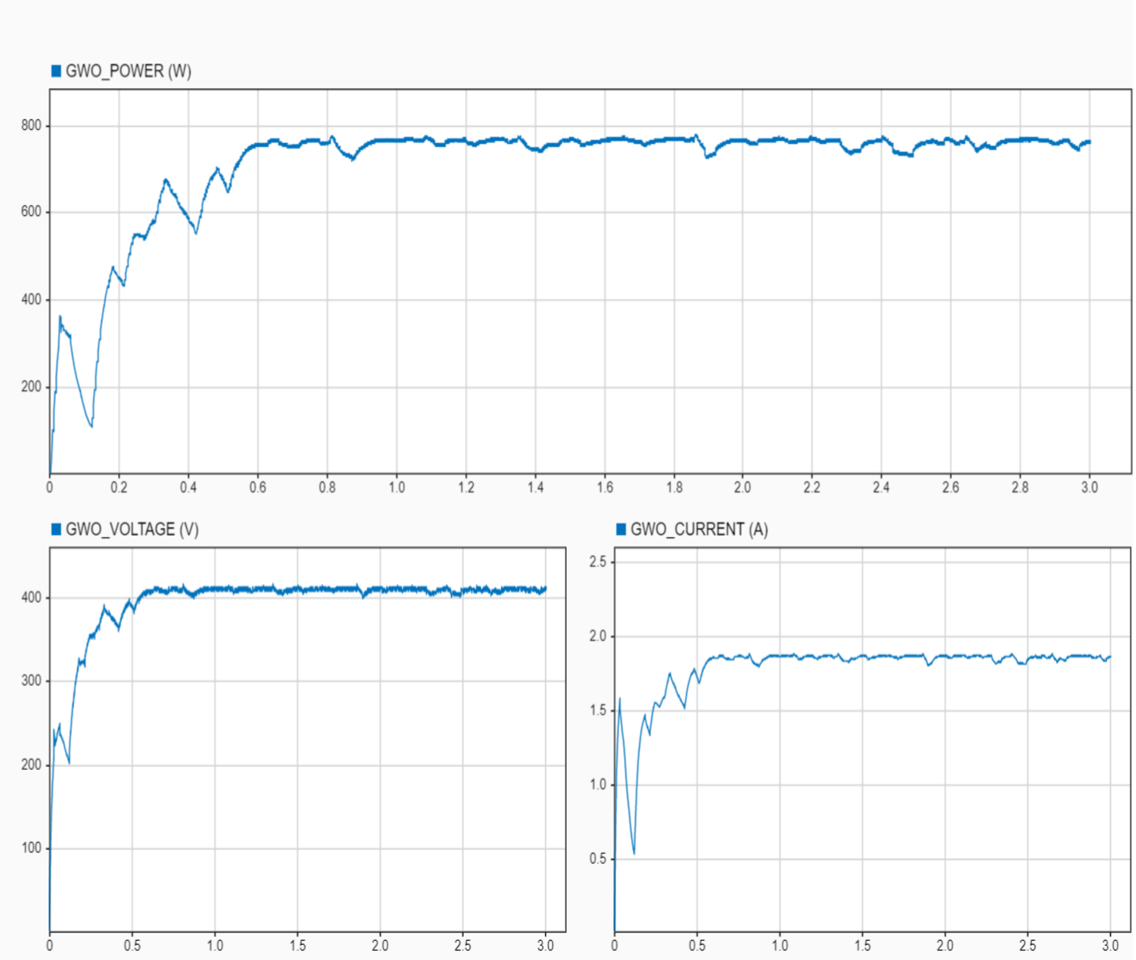

Figure 4.11. Dynamic PV performance of the proposed system under partial shading conditions using GWO algorithm

Initially, the PV power, voltage, and current exhibit significant adjustements with values fluctuating considerably, before settling into a more stable pattern at 0.6 seconds and acheiving 777.5 W of output power. This results, indicate that the global maximum power point has been succefully tracked, showing the GWO algorithm's robustness in managing partial shading conditions and maintaining the maximum power output.

- **Performance of Synchronous BLDC Motor Pump**

The Figure 4.12 displays the rotor speed W_m, load torque T_L, and electromagnetic torque T_e under variable irradiance using grey wolf optimization algorithm.

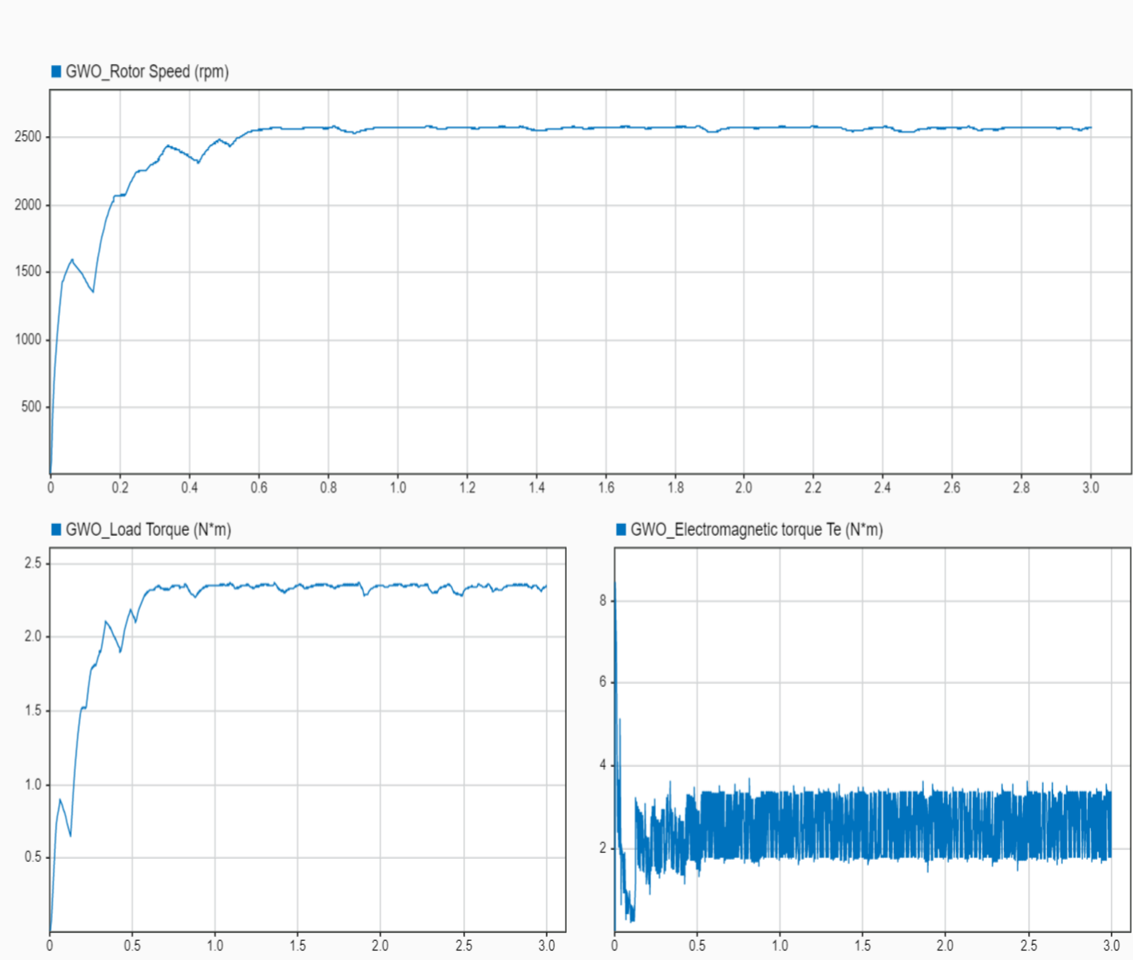

Figure 4.12. Dynamic BLDC motor performance of the proposed system under partial shading conditions using GWO algorithm

The rotor speed W_m and load torque T_L graphs experience initial fluctuations that can be attributed to the adjustments made by the GWO algorithm, then they stabilize at 0.6 seconds reaching the values of 2528.5 rpm, and 2.36 N*m, respectively. However, minor oscillations could be observed around their steady-state values. Similarly, the electromagnetic torque T_e graph shows a rapid increase and then maintains a steady state with notable noise levels.

4.3.2.4 Steady State and Starting Performances Using MPA

• Performance of SPV Array

The Figure 4.13 below illustrates the PV power, voltage, and current under partial shading conditions, optimized using the Marine Predator algorithm.

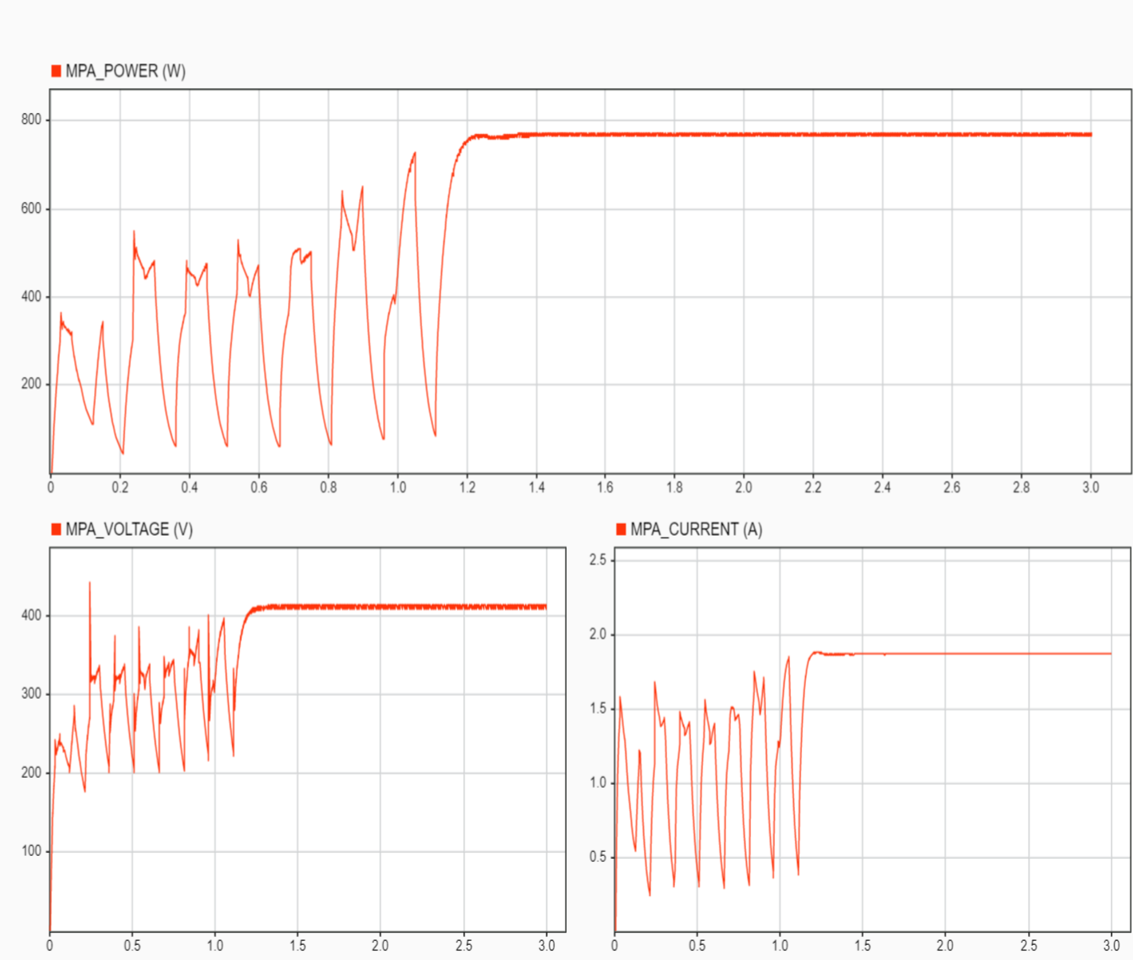

Figure 4.13. Dynamic PV performance of the proposed system under partial shading conditions using MPA

In terms of convergence time, all three parameters exhibit rapid initial oscillations, the stabilizes after about 1.23 seconds, reflecting the active adjustments made by the MPA. Furthermore, The PV power achieved steady-state value of 772.3 W, demonstrating the proficiency of MPA in tracking the global maximum power point (GMPP). Hence, optimizing the PV system's performance.

- **Performance of Synchronous BLDC Motor Pump**

The Figure 4.14 displays the rotor speed W_m, load torque T_L, and electromagnetic torque T_e under variable irradiance using grey wolf optimization algorithm.

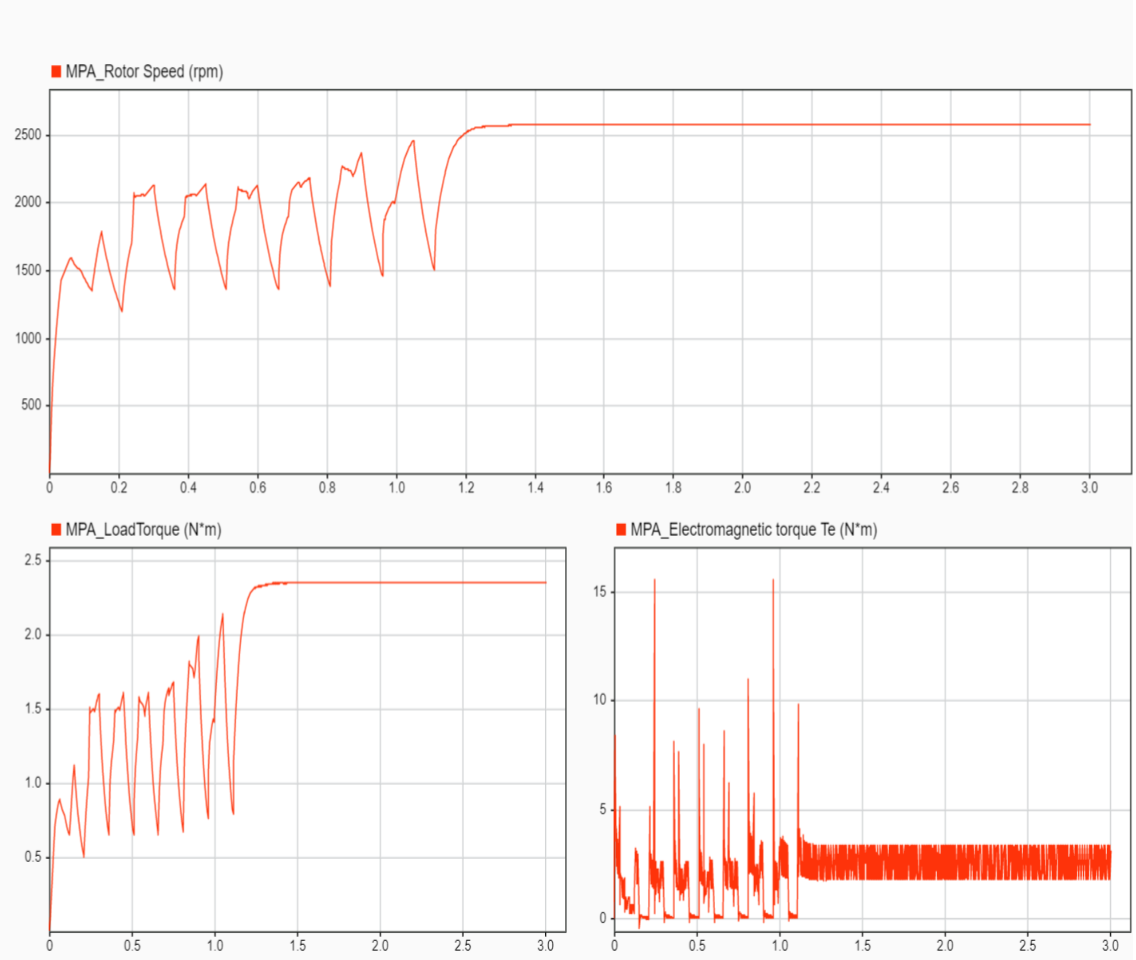

Figure 4.14. Dynamic BLDC motor performance of the proposed system under partial shading conditions using MPA

The rotor speed W_m graph shows significant oscillations at the begining, reflecting the MPA's dynamic adjustments, but it stabilizes around 1.23 seconds, reaching a steady state of 2581.5 rpm. The load torque T_e graph exhibits similar oscillatory behavior at the beginning, indicating the system's adaptation process, but it eventually stabilizes at around 2.36 N*m, aligning with the rotor speed's stabilization time. However, the electromagnetic torque T_e graph initially displays considerable fluctuations, which gradually reduce as the system approaches stability, demonstrating the MPA's effort to optimize the system's performance.

4.4 Comparison and Discussion

The following Figure 4.15, combines the dynamic response of the used algorithm in terms of power output, rotor speed W_m, and load torque T_L over time under partial shading.

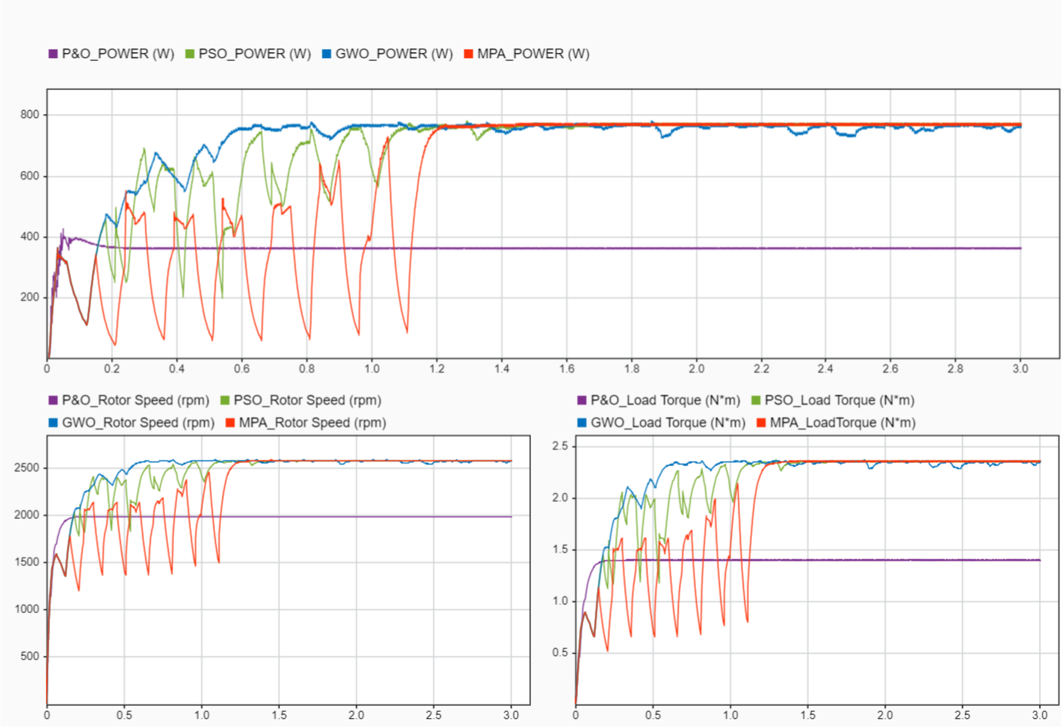

Figure 4.15. Combined power output, rotor speed W_m, and load torque T_L of the used algorithms under partial shading conditions

The table 4.1 summarizes the key performance, including convergence time, MPP tracking capability, steady-state noise, output power, rotor speed W_m, and load torqueT_L. Where, the global maximum power point (GMPP) of our solar water pumping system under partial shading conditions noted to be 784 W.

Table 4.1. Comparison of P&O, PSO, GWO, and MPA algorithms under partial shading conditions

Algorithm	**Convergence Time (S)**	**MPP Tracking**	**Steady-State Noise**	**Power (W)**	**Rotor speed W_m (rpm)**	**Load torque T_L (N*m)**
P&O	Fast (0.5)	Does not reach global MPP	Minimal	363.9	1987.1	1.39
PSO	Moderate (1.4)	Reaches global MPP	Noticeable	771.8	2588.4	2.37
GWO	Fast (0.6)	Reaches global MPP	Moderate	777.5	2528.5	2.36
MPA	Moderate (1.23)	Reaches global MPP	Minimal	772.3	2581.5	2.36

According to the results illustrated in Figure 4.15 and summarized in table 4.1, it is evident that among all the four used algorithms, only PSO, GWO, and MPA effectively reach the global MPP of 784 W, with their power outputs being 771.8 W, 777.5 W, and 772.3 W, respectively. The P&O algorithm, despite its fast convergence, fails to reach the global MPP, achieving only 363.9 W. Moreover, the PSO algorithm exhibits noticeable steady-state noise, while the MPA algorithm achieves minimal noise, making it a balanced choice for efficient and stable performance under partial shading conditions. The rotor speed W_m and load torque T_L graphs reveal that P&O maintains stable but could not reach desired values, while PSO, GWO, and MPA exhibit initial oscillations before stabilizing, with MPA achieving a rotor speed of 2581.5 rpm and load torque of 2.36 N*m. The table further highlights that while P&O has minimal steady-state noise, it does not reach the GMPP. In contrast, PSO and GWO show noticeable and moderate steady-state noise, respectively, with MPA achieving minimal noise and effectively balancing fast convergence and optimal power tracking.

4.5 Conclusion

In this chapter, we examined simulation results and performance analysis of our solar water pumping system. We started by detailing the system's basic characteristics, then moved on to simulate its behavior using the P&O algorithm under different irradiance levels. We also tested the system's performance under shading conditions with four different algorithms including, P&O, GWO, PSO, and MPA. Finally, we compared these algorithms, discussing their results in terms of how quickly they converge, their MPP tracking accuracy, noise levels, output power, rotor speed W_m, and load torque T_L. This comparaison provided valuable perspectives into which MPPT algortihm is the best for our solar water pumping system.

General Conclusion

This report has provided a comprehensive exploration of solar water pumping systems (SWPS), highlighting their potential as a solution for water management in various applications. Starting with the state of the art in solar energy and SWPS technology, we reviewed the essential components and configurations, including the types of power sources, pumps, and motors used. The maximum power point tracking (MPPT) algorithms were discussed in detail, with a focus on their performance under different environmental conditions, including partial shading.

In the system configuration and description section, we examined the photovoltaic (PV) arrangements, including the characteristics and modeling of PV cells, modules, and arrays. The impact of variations in solar irradiation and temperature on PV performance was analyzed, along with the roles of DC-DC boost converter and three-phase VSI inverter. We also delved into the operational principle and dynamic modeling of brushless DC motors and centrifugal pumps, which are important components of SWPS.

The maximum power point tracking techniques, including traditional ones such perturb and observe (P&O) and metaheuristic algorithms such as Particle Swarm Optimization (PSO), Grey Wolf Optimization (GWO), and Marine Predator Algorithm (MPA), were evaluated for their effectiveness in optimizing the power output of solar panels.

Finally, the simulation results and discussion section presented an detailed analysis of the system's characteristics and performance. The output power, steady-state and starting performances of used MPPT algorithms were compared, demonstrating the efficacy of advanced optimization techniques in enhancing the efficiency of SWPS.

Future Work

- Perform some practical experiments to verify the obtained simulation results.

- Developing another metaheuristic MPPT algorithm to the system.

- Extend the current work by incorporating multilevel inverters to reduce the switching losses in the three-phase VSI inverter system.

A. Appendix

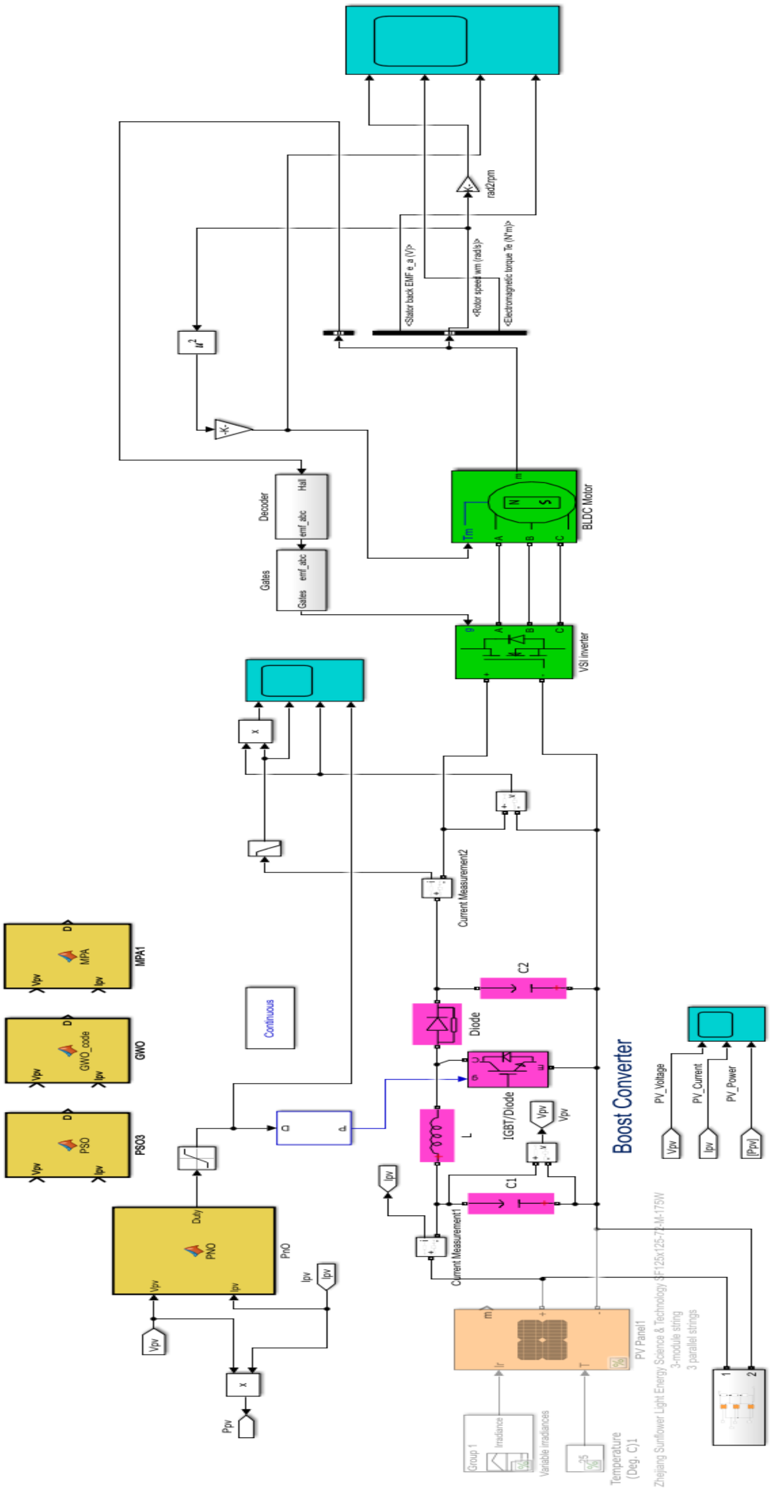

Figure A.1. Global simulation model

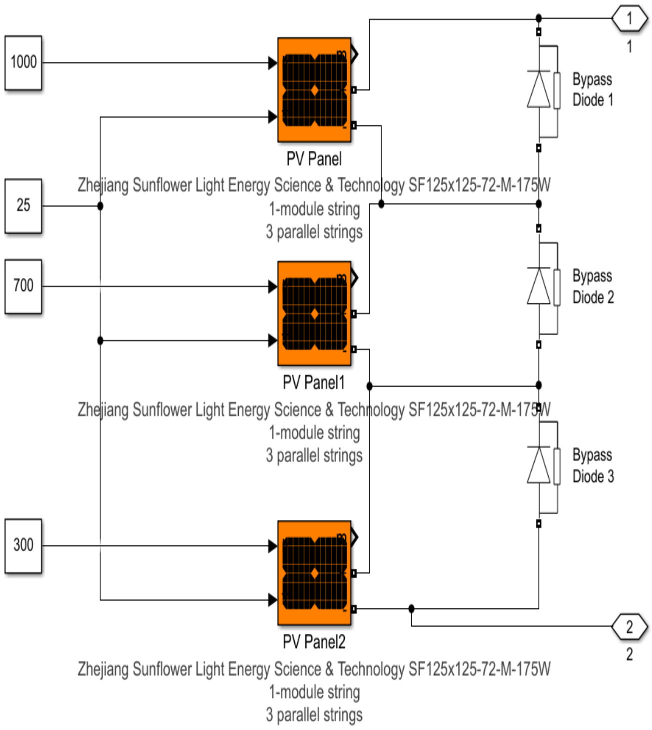

Figure A.2. Configuration of PV Panels Under Partial Shading Conditions

Table A.1. BLDC motor parameters

Design Parameters	Value
Rated Torque T_d	4.2 Nm
Rated Power P_d	1.35 kW
Rated Speed N_r	2880rpm
Poles N_m	10
Phase Resistance R_{ph}	0.7 Ω
Phase inductance L_{ph}	4mH
Torque constant K_t	0.7 Nm/A
Moment of Inertia J	0.0028 kg/m^3

Table A.2. Boost parameters

Element	Rating
Input capacitor C_1	9 e-4 F
Inductor L	9.9 e-6 H
Output capacitor C_2	7 e-5 F

References

[1] Ricardo Luna-Rubio et al. "Optimal sizing of renewable hybrids energy systems: A review of methodologies". In: *Solar energy* 86.4 (2012), pp. 1077–1088.

[2] AK Akella, RP Saini, and Mahendra Pal Sharma. "Social, economical and environmental impacts of renewable energy systems". In: *Renewable energy* 34.2 (2009), pp. 390–396.

[3] JS Ramos and Helena M Ramos. "Solar powered pumps to supply water for rural or isolated zones: A case study". In: *Energy for Sustainable Development* 13.3 (2009), pp. 151–158.

[4] Nabil Karami, Nazih Moubayed, and Rachid Outbib. "General review and classification of different MPPT Techniques". In: *Renewable and Sustainable Energy Reviews* 68 (2017), pp. 1–18.

[5] Hamza Belmadani et al. "A New Fast and Efficient MPPT Algorithm for Partially Shaded PV Systems using a Hyperbolic Slime Mould Algorithm". In: *International Journal of Energy Research* (Jan. 2024). DOI: `10.1155/2024/5585826`.

[6] Jeff Kenna and Bill Gillett. "Solar water pumping. A handbook". In: (1985).

[7] Hala J El-Khozondar et al. "A review study of photovoltaic array maximum power tracking algorithms". In: *Renewables: Wind, Water, and Solar* 3 (2016), pp. 1–8. DOI: `http://dx.doi.org/10.1186/s40807-016-0022-8`.

[8] Belkacem Bouzidi. "New sizing method of PV water pumping systems". In: *Sustainable Energy Technologies and Assessments* 4 (2013), pp. 1–10. DOI: `https://doi.org/10.1016/j.seta.2013.08.00`.

[9] Arunendra K Tiwari et al. "Effect of head and PV array configurations on solar water pumping system". In: *Materials Today: Proceedings* 46 (2021), pp. 5475–5481. DOI: `10.1016/j.matpr.2020.09.200`.

[10] JK Kaldellis, E Meidanis, and D Zafirakis. "Experimental energy analysis of a stand-alone photovoltaic-based water pumping installation". In: *Applied Energy* 88.12 (2011), pp. 4556–4562.

[11] Vimal Chand Sontake and Vilas R Kalamkar. "Solar photovoltaic water pumping system-A comprehensive review". In: *Renewable and Sustainable Energy Reviews* 59 (2016), pp. 1038–1067.

[12] Robert Foster and Alma Cota. "Solar water pumping advances and comparative economics". In: *Energy Procedia* 57 (2014), pp. 1431–1436.

[13] Rosa J Chilundo, Diana Neves, and Urânio S Mahanjane. “Photovoltaic water pumping systems for horticultural crops irrigation: Advancements and opportunities towards a green energy strategy for Mozambique”. In: *Sustainable Energy Technologies and Assessments* 33 (2019), pp. 61–68. DOI: `https://doi.org/10.1016/j.seta.2019.03.004`.

[14] Rajan Kumar and Bhim Singh. “Solar PV-battery based hybrid water pumping system using BLDC motor drive”. In: *2016 IEEE 1st International Conference on Power Electronics, Intelligent Control and Energy Systems (ICPEICES)*. IEEE. 2016, pp. 1–6.

[15] “SOLAR WATER PUMPING SYSTEMS DESIGN, SELECTION AND INSTALLATION GUIDELINES”. In: *Guideline of The Pacific Power Association (PPA).*

[16] Rajan Kumar and Bhim Singh. “BLDC motor-driven solar PV array-fed water pumping system employing zeta converter”. In: *IEEE Transactions on Industry Applications* 52.3 (2016), pp. 2315–2322.

[17] Djamila Rekioua and Ernest Matagne. *Optimization of photovoltaic power systems: modelization, simulation and control*. Springer Science & Business Media, 2012.

[18] Abdelilah Hilali et al. “Migration to solar water pump system: Environmental and economic benefits and their optimization using genetic algorithm Based MPPT”. In: *Energy Reports* 8 (2022), pp. 10144–10153.

[19] Siva Ganesh Malla, CN Bhende, and S Mishra. “Photovoltaic based water pumping system”. In: *2011 International Conference on Energy, Automation and Signal*. IEEE. 2011, pp. 1–4.

[20] M Masters Gilbert. *Renewable and efficient electric power systems*. John Wiley & Sons, 2004.

[21] Md Rabiul Islam et al. “Simulation of PV array characteristics and fabrication of microcontroller based MPPT”. In: *International Conference on Electrical & Computer Engineering (ICECE 2010)*. IEEE. 2010, pp. 155–158.

[22] Sudha Bansal, Lalit Mohan Saini, and Dheeraj Joshi. “Design of a DC-DC converter for photovoltaic solar system”. In: *2012 IEEE 5th India International Conference on Power Electronics (IICPE)*. IEEE. 2012, pp. 1–5.

[23] K Rahrah et al. “Photovoltaic pumping system in Bejaia climate with battery storage”. In: *International journal of hydrogen energy* 40.39 (2015), pp. 13665–13675.

[24] Eduardo Roman et al. “Intelligent PV module for grid-connected PV systems”. In: *IEEE Transactions on Industrial electronics* 53.4 (2006), pp. 1066–1073.

[25] H Rashid Muhammad. “Power Electronics-Circuits, Devices, and Applications”. In: *Upper Saddle River, NJ, Pearson Prentice Hall* (2004).

[26] Santanu Mondal, Arunabha Mitra, and Madhurima Chattopadhyay. “Mathematical modeling and simulation of Brushless DC motor with ideal Back EMF for a precision speed control”. In: *2015 IEEE International Conference on Electrical, Computer and Communication Technologies (ICECCT)*. IEEE. 2015, pp. 1–5.

[27] Milan Brejl, Michal Princ, and Pavel Sustek. “BLDC Motor with Hall Sensors and Speed Closed Loop, Driven by eTPU on MPC5554”. In: (2006).

[28] Y Narendra Kumar et al. “Speed Control of BIdc Motor Drive By Using PID Controllerǁ”. In: *International Journal of Engineering Research and Applications* 4.4 (2014), pp. 37–41.

[29] Salim Djeriou, Aissa Kheldoun, and Adel Mellit. “Efficiency improvement in induction motor-driven solar water pumping system using golden section search algorithm”. In: *Arabian Journal for Science and Engineering* 43.6 (2018), pp. 3199–3211.

[30] Laxman Bhukya and Srikanth Nandiraju. “A novel photovoltaic maximum power point tracking technique based on grasshopper optimized fuzzy logic approach”. In: *International journal of hydrogen energy* 45.16 (2020), pp. 9416–9427.

[31] Ekrem Kandemir, Numan S Cetin, and Selim Borekci. “A comprehensive overview of maximum power extraction methods for PV systems”. In: *Renewable and sustainable energy reviews* 78 (2017), pp. 93–112.

[32] Nicola Femia et al. “Optimization of perturb and observe maximum power point tracking method”. In: *IEEE transactions on power electronics* 20.4 (2005), pp. 963–973.

[33] Rozana Alik, Awang Jusoh, and Tole Sutikno. “A review on perturb and observe maximum power point tracking in photovoltaic system”. In: *TELKOMNIKA (Telecommunication Computing Electronics and Control)* 13.3 (2015), pp. 745–751.

[34] Santiago Silvestre and A Chouder. “Effects of shadowing on photovoltaic module performance”. In: *Progress in Photovoltaics: Research and applications* 16.2 (2008), pp. 141–149.

[35] Hegazy Rezk and Ali M Eltamaly. “A comprehensive comparison of different MPPT techniques for photovoltaic systems”. In: *Solar energy* 112 (2015), pp. 1–11.

[36] Young-Hyok Ji et al. “A real maximum power point tracking method for mismatching compensation in PV array under partially shaded conditions”. In: *IEEE Transactions on power electronics* 26.4 (2010), pp. 1001–1009.

[37] Suneel Raju Pendem and Suresh Mikkili. “Modeling, simulation and performance analysis of solar PV array configurations (Series, Series–Parallel and Honey-Comb) to extract maximum power under Partial Shading Conditions”. In: *Energy Reports* 4 (2018), pp. 274–287.

[38] Mohammad Reza Maghami et al. “Power loss due to soiling on solar panel: A review”. In: *Renewable and Sustainable Energy Reviews* 59 (2016), pp. 1307–1316.

[39] Qinghai Bai. “Analysis of particle swarm optimization algorithm”. In: *Computer and information science* 3.1 (2010), p. 180.

[40] Seyedali Mirjalili, Seyed Mohammad Mirjalili, and Andrew Lewis. “Grey wolf optimizer”. In: *Advances in engineering software* 69 (2014), pp. 46–61.

[41] Afshin Faramarzi et al. “Marine Predators Algorithm: A nature-inspired metaheuristic”. In: *Expert systems with applications* 152 (2020), p. 113377.

[42] Nicolas E Humphries et al. “Environmental context explains Lévy and Brownian movement patterns of marine predators”. In: *Nature* 465.7301 (2010), pp. 1066–1069.

[43] Mahmoud A Soliman, Hany M Hasanien, and Abdulaziz Alkuhayli. “Marine predators algorithm for parameters identification of triple-diode photovoltaic models”. In: *IEEE Access* 8 (2020), pp. 155832–155842.